J Neurophysiol 91: 2322–2329, 2004.
First published December 24, 2003; 10.1152/jn.01049.2003.

Small-Conductance Ca^{2+}-Dependent K^+ Channels Are the Target of Spike-Induced Ca^{2+} Release in a Feedback Regulation of Pyramidal Cell Excitability

Shin-Ichiro Yamada,[1,2], Hajime Takechi,[1], Izumi Kanchiku,[1], Toru Kita,[2], and Nobuo Kato[3],
Departments of [1]Geriatric Medicine, [2]Cardiovascular Medicine, and [3]Integrative Brain Science, Kyoto University Graduate School of Medicine, Kyoto 606-8501, Japan

Submitted 30 October 2003; accepted in final form 17 December 2003

Yamada, Shin-Ichiro, Hajime Takechi, Izumi Kanchiku, Toru Kita, and Nobuo Kato. Small-conductance Ca^{2+}-dependent K^+ channels are the target of spike-induced Ca^{2+} release in a feedback regulation of pyramidal cell excitability. *J Neurophysiol* 91: 2322–2329, 2004. First published December 24, 2003; 10.1152/jn.01049.2003. Cooperative regulation of inosiol-1,4,5-trisphosphate receptors (IP_3Rs) by Ca^{2+} and IP_3 has been increasingly recognized, although its functional significance is not clear. The present experiments first confirmed that depolarization-induced Ca^{2+} influx triggers an outward current in visual cortex pyramidal cells in normal medium, which was mediated by apamin-sensitive, small-conductance Ca^{2+}-dependent K^+ channels (SK channels). With IP_3-mobilizing neurotransmitters bath-applied, a delayed outward current was evoked in addition to the initial outward current and was mediated again by SK channels. Calcium turnover underlying this biphasic SK channel activation was investigated. By voltage-clamp recording, Ca^{2+} influx through voltage-dependent Ca^{2+} channels (VDCCs) was shown to be responsible for activating the initial SK current, whereas the IP_3R blocker heparin abolished the delayed component. High-speed Ca^{2+} imaging revealed that a biphasic Ca^{2+} elevation indeed underlays this dual activation of SK channels. The first Ca^{2+} elevation originated from VDCCs, whereas the delayed phase was attributed to calcium release from IP_3Rs. Such enhanced SK currents, activated dually by incoming and released calcium, were shown to intensify spike-frequency adaptation. We propose that spike-induced calcium release from IP_3Rs leads to SK channel activation, thereby fine tuning membrane excitability in central neurons.

INTRODUCTION

Intracellular Ca^{2+} is a versatile second messenger in neurons. Varieties of neural events such as long-term potentiation (Berridge 1998; Lynch et al. 1983), long-term depression (Rose and Konnerth 2001; Sakurai 1990), electroencephalographic (EEG) rhythm generation (McCormick and Contreras 2001), and neural cell death (Choi 1995) are all dependent on intracellular Ca^{2+} increase. Yet, once intracellular Ca^{2+} is increased, one of such Ca^{2+}-dependent events, but not the others, is specifically triggered. How can the versatility and specificity co-exist in the neural Ca^{2+} signaling? An emerging view related to this question is that Ca^{2+} channels and Ca^{2+}-activated channels form functional complexes, and each complex may be dedicated to one particular function. It is classically known that a channel coupling composed of voltage-dependent Ca^{2+} channels (VDCCs) and small-conductance Ca^{2+}-dependent K^+ channels (SK channels) is responsible for spike-frequency adaptation, a Ca^{2+}-dependent negative feedback regulation of membrane excitability (Sah 1996). A specific linkage of *N*-methyl-D-aspartate receptors (NMDARs) and large-conductance Ca^{2+}-dependent K^+ channels (big-K; BK channels) enables a synaptically triggered, extra-synaptic inhibition (Isaacson and Murphy 2001). Ca^{2+} inflow from NMDARs is known as a particularly suitable activator of ryanodine receptors (RyRs) in hippocampus pyramidal cell spines, suggesting a functional coupling between NMDARs and RyRs (Emptage et al. 1999). An intimate link is proposed between VDCCs and Ca^{2+}-dependent cationic channels, which contributes to generation of spike afterdepolarization (Partridge and Valenzuela 1999). The Ca^{2+}-activated Ca^{2+}-release channels RyRs and IP_3Rs appear to play unique roles in organizing such channel complex because these channels can be targets and donors of Ca^{2+} at the same time. Hence, the Ca^{2+} release from these channels may in turn activate a second target, thereby forming a functional triad instead of a coupling.

An interesting feature of such a functional triad involving inosiol-1,4,5-trisphosphate receptors (IP_3Rs) would be that the intermediate member of the triad, the IP_3R, is dependent not just on Ca^{2+} but also on IP_3-mobilizing neurotransmitters. Recently, cooperative regulation of IP_3Rs by Ca^{2+} and IP_3 (Bezprozvanny et al. 1991; Finch et al. 1991; Iino 1990) has been increasingly recognized in neurons (Nakamura et al. 1999, 2000; Wang et al. 2000; Yamamoto et al. 2000, 2002a,b; Yang et al. 2002). Typically, a Ca^{2+}-induced Ca^{2+} release (CICR) from IP_3Rs has been described in hippocampus (Nakamura et al. 1999; Power and Sah 2002) and visual cortex pyramidal cells (Yamamoto et al. 2000) in which IP_3Rs are activated beforehand by IP_3 until their opening is finally triggered by action potential-induced Ca^{2+} inflow through VDCCs. We have proposed that a functional significance of this mode of IP_3-assisted CICR may reside in its role in enhancement of spike-frequency adaptation (Yamamoto et al. 2002a). Because the target of this distinct type of CICR is not known, a functional triad consisting of VDCCs, IP_3Rs, and the yet-unknown target has not been undoubtedly established to date. We have now identified SK channels as the target. This functional triad was switched on by IP_3-mobilizing neurotransmitters and indeed enhanced spike-frequency adaptation in visual cortex pyramidal cells.

Address for reprint requests and other correspondence: N. Kato, Dept. of Integrative Brain Science, Graduate School of Medicine, Kyoto University, 606-8501 Kyoto, Japan (E-mail: f50207@sakura.kudpc.kyoto-u.ac.jp).

The costs of publication of this article were defrayed in part by the payment of page charges. The article must therefore be hereby marked "*advertisement*" in accordance with 18 U.S.C. Section 1734 solely to indicate this fact.

METHODS

Slice preparation

All experiments were performed in accordance with the guiding principle of the Physiological Society of Japan and with the approval of the Animal Care Committee of Kyoto University Graduate School of Medicine. Slices (300 μm thick) of the visual cortex were prepared from Wistar rats (16–18 days old) with a microslicer DTK-1000 (Dosaka, Kyoto, Japan). Slices were kept at room temperature for ≥60 min before experiments in normal medium composed (in mM) of 124 NaCl, 3.0 KCl, 2.5 $CaCl_2$, 2.5 $MgSO_4$, 1.3 NaH_2PO_4, 26 $NaHCO_3$, and 10 glucose bubbled with a mixture of 95% O_2-5% CO_2. In some experiments, CNQX (10 μM) and bicuculline (10 μM) were added. The slices were placed in a recording chamber on the stage of an upright microscope (BX50WI, Olympus, Tokyo, Japan) with a ×60 water-immersion objective. The chamber was continuously perfused with medium at room temperature (~25°C) bubbled with a mixture of 95% O_2-5% CO_2.

Electrophysiology

Whole cell recordings were made from the soma of visually identified pyramidal neurons located in layer 2/3 of the visual cortex. Recordings were continued only in cells that had the resting membrane potential below −55 mV. Patch pipettes (5–8 MΩ) were filled with an internal solution containing (in mM) 7 KCl, 144 K-gluconate, 10 HEPES, 2 MgATP, and 0.2 Na_2GTP, pH adjusted to 7.3 with KOH. Capacitance was compensated almost fully. Series resistance was always 15–50 MΩ and left uncompensated. The EPC-9 patch-clamp amplifier and program package PULSE-PULSEFIT (HEKA Electronics, Lambrecht, Germany) were used for data acquisition. For voltage-clamp recording (held at −55 mV), a short depolarization command to +10 mV for 5 ms was applied to evoke tail currents (I_{AHP}), which would generate afterhyperpolarization (AHP) under current clamp (I_{AHP}). I_{AHP}s were recorded every 40–60 s and digitized at 5–10 kHz. We integrated I_{AHP} from 20 to 200–500 ms after the step depolarization to calculate the charge transfer representing the medium AHP (mAHP). This charge transfer was adopted as the index for evaluating the magnitude of mAHPs. For current-clamp recording, a single action potential was evoked by a 3-ms depolarization current pulse (800 pA), and mAHP following the action potential was recorded. Trains of action potentials were evoked by injecting depolarizing currents (100–250 pA for 500 ms). Carbachol application depolarized recorded neurons by at most 5–10 mV, and we set the membrane potential back exactly to the resting level by passing hyperpolarizing currents. The current-clamp recording started 5 min after the application.

Drugs used

Depending on the purpose of experiments, we bath-applied one or more of the following drugs: apamin (100 nM; Alomone), carbachol (Cch; 10 μM), atropine (1 μM), thapsigargin (1 μM; Alomone), (RS)-3,5-dihydroxyphenylglycine (DHPG; 10 μM; Tocris), CNQX (10 μM; Tocris) and bicuculline (10 μM; Tocris), linopirdine (50 μM; Sigma), iberiotoxin (50 nM; Alomone). Heparin (low molecular weight, 4 mg/ml; Calbiochem) and ruthenium red (100 μM) were contained in the internal solution of patch pipettes and thereby injected intracellularly. For thapsigargin application, the recorded cells were preincubated for 20–60 min in medium containing thapsigargin. For Ca^{2+} imaging, the Ca^{2+} indicator Oregon Green 488 BAPTA-1 (50 μM; Molecular Probe) was injected intracellularly. Ni^{2+} (500 μM) was applied extracellularly. At this concentration, Ni^{2+} blocks all subtypes of VDCCs (Randall 1998). All the drugs were purchased from Nacalai (Kyoto, Japan) unless otherwise noted.

Ca^{2+} imaging

For Ca^{2+} imaging, neurons were filled with Oregon green 488 BAPTA-1 (50 μM), a Ca^{2+} indicator, through the patch pipette. Fluorescence images were acquired by a high-speed confocal laser-scanning microscope (Oz, Noran). Based on the fluorescence image, the time course of fluorescence intensity was calculated in several regions of interest (ROIs), which were selected over the nucleus (N), extranuclear soma (S), and the proximal dendrite (D). To examine Ca^{2+} transients in response to the depolarization command, 150 or 200 frames of image were collected at 120 Hz, and the increase in fluorescence intensity was averaged over each ROI within images. The fluorescence signals were subjected to background correction and were expressed as relative increases in fluorescence ($\Delta F/F$) in comparison with the prestimulus fluorescence level (F). Recorded cells were held at −55 mV, and a depolarization step to +10 mV for 5 ms was given for each recording session.

Date analysis

Recorded data were analyzed with StatView. Data are expressed as means ± SE. Paired or unpaired t-test was used for statistics with the significance level set at $P < 0.05$.

RESULTS

Delayed I_{AHP} component induced by mAchR activation

Under voltage clamp, the current that would produce AHP under current clamp (I_{AHP}) was elicited in pyramidal neurons by a depolarization pulse. I_{AHP} was integrated from 20 to 200 or 500 ms after the pulse termination to calculate the charge transfer carried by the middle part of I_{AHP} that corresponds to the medium AHP (mAHP) (Sah 1996). I_{AHP} had a single peak followed by a single exponential decay, which lasted ~200 ms. I_{AHP} was completely abolished by the selective SK channel antagonist apamin (Fig. 1*A*), thus reflecting mostly mAHP. The charge transfer was reduced to 7.1 ± 3.8% ($n = 8$, $P < 0.0001$) by apamin, confirming that I_{AHP} was attributable largely to SK channels. After application of the muscarinic agonist Cch, a second slow component of I_{AHP} emerged after the same fast component as observed without Cch, thereby enhancing the total charge transfer to 297 ± 21% ($n = 40$, $P < 0.0001$; Figs. 1*B* and 2). By co-application of apamin along with Cch, both the fast and slow components of I_{AHP} were completely abolished (−44.2 ± 7.7%, $n = 15$, $P < 0.0001$). In the presence of Cch and apamin, but not with apamin alone, a small, sustained inward current was observed after the depolarization pulse (Figs. 1*B* and 2). Co-application of the muscarinic receptor (mAchR) antagonist atropine with Cch completely prevented the Cch-induced emergence of the slow component, which is evidenced by reduction of the slow I_{AHP} enhancement to 98.9 ± 1.1% ($n = 7$, Figs. 1*C* and 2) as compared with 297 ± 21% in the presence of Cch alone ($P < 0.001$).

Ca^{2+} mobilization underlying the dual I_{AHP} activation

What role does the Ca^{2+} influx through VDCCs play in the dual activation of I_{AHP}? Removal of the extracellular Ca^{2+} almost completely abolished both the fast and slow activations (Figs. 1*D* and 2). The charge transfer by I_{AHP} was reduced to 15.9 ± 9.3% ($n = 9$, $P < 0.0001$) of control. I_{AHP} was also sensitive to VDCC blockade by 500 μM Ni^{2+} with the charge transfer reduced to 5.0 ± 8.1% ($n = 10$, $P < 0.0001$, Fig. 2).

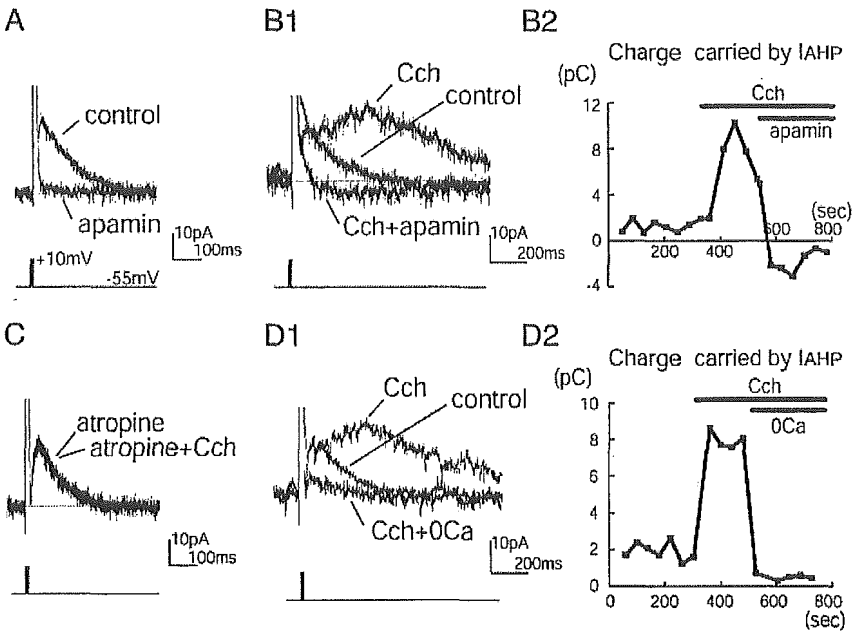

FIG. 1. Emergence of a delayed, slow component of apamin-sensitive I_{AHP} in carbachol (Cch)-containing medium. *A*: I_{AHP} with a simple time course was evoked in control medium and blocked completely by apamin. *B1*: a delayed component of I_{AHP} appeared after Cch application. Both the initial and delayed components were abolished by apamin. *B2*: time course of the drug effects on the charge transfer from the start of recording ($t = 0$). Each drug was bath-applied during the time span indicated by the bar. *C*: atropine prevented the effect of Cch. *D, 1* and *2*: the Cch-dependent delayed component (Cch), as well as the initial one (control), was abolished in Ca^{2+}-free medium (0 Ca).

These results indicate that Ca^{2+} influx through VDCCs is essential for generating both the fast and the Cch-induced, slow components of I_{AHP}.

How did the slow I_{AHP} component emerge with Cch application? Because mAchR activation by Cch will produce IP_3, Ca^{2+} released through IP_3R may keep SK channels activated for a longer period. To test this possibility, the IP_3R blocker heparin was included in the patch solution. Heparin prevented the slow enhancement of I_{AHP} in all the cells tested (67.3 ± 4.9%, $n = 9$, $P < 0.0001$; Fig. 3, *A* and *D*). Thapsigargin, a Ca^{2+} store depleter, also prevented this slow enhancement (67.3 ± 4.9%, $n = 9$, $P < 0.0001$; Fig. 3, *B* and *D*). Because Ca^{2+} influx might activate RyRs as well, we tested the effect of ruthenium red, a blocker of RyRs. But, the enhancement of I_{AHP} due to Cch was 280 ± 44% with ruthenium red ($n = 4$, $P < 0.0001$; Fig. 3, *C* and *D*), which was not significantly different from the 297 ± 21% increase with Cch alone. These results indicate that Ca^{2+} release from IP_3Rs, but not RyRs, is essential for emergence of the slow enhancement of I_{AHP}. IP_3 is produced by activation of type I metabotropic glutamate receptors (mGluRs) as well. The potent type-I-mGluR agonist DHPG indeed enhanced I_{AHP} (to 356 ± 40%, $n = 8$, $P < 0.0001$; Fig. 3*E*), indicating that increase in IP_3 is essential and sufficient for the slow activation of SK channels.

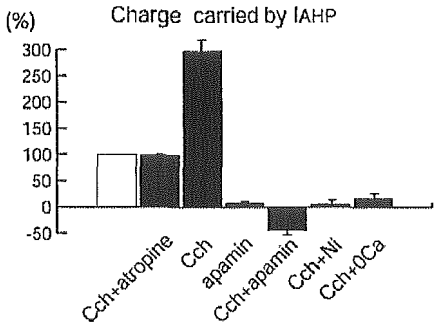

FIG. 2. Across-group comparison of the I_{AHP}-carried charge. The charge transfer, expressed as percent of controls, was increased by Cch application (Cch), and reduced by applying apamin. The effect of Cch was cancelled out by atropin (Cch + atropin). Both the effect of Cch and the control charge transfer were eliminated by applying apamin alone (apamin) or in combination with Cch (Cch + apamin), by nominally removing extracellular Ca^{2+} (Cch + 0 Ca), or by blocking voltage-dependent Ca^{2+} channels (VDCCs, Cch + Ni).

Imaging study of Ca^{2+} mobilization

By Ca^{2+} imaging, Ca^{2+} mobilization underlying the dual SK channel activation was investigated (Fig. 4). Prior to Cch application, $[Ca^{2+}]_i$ elevation occurred immediately after the depolarization command and decreased gradually both in soma and proximal dendrite, thus consisting of just one phase of increase (Fig. 4*C*, black lines). This was observed in all the three ROIs (N, S, D in Fig. 4, *A* and *C*). After Cch application, by contrast, a delayed phase of $[Ca^{2+}]_i$ increase emerged and overrode the initial phase in all the ROIs (Fig. 4*C*, red lines). The green lines in Fig. 4*C* indicate the subtractions between $[Ca^{2+}]_i$ elevations with and without Cch, thus representing the newly emerged phase of $[Ca^{2+}]_i$ increase after Cch application. Ca^{2+} increases at the peak of elevation, as expressed by percent of the prepulse level ($\Delta F/F$), were 44.3 ± 7.1% (N), 93.3 ± 10.4% (S), and 167.4 ± 14.9% (D) after Cch application, and significantly greater than before Cch application (N, 17.7 ± 1.1%, $P < 0.005$; S, 57.0 ± 8.1%, $P < 0.0005$; D, 124.2 ± 15.0%, $P < 0.005$; $n = 12$).

The Cch-dependent slow component was completely abolished by intracellular application of heparin, and is therefore likely to reflect depolarization-induced Ca^{2+} release from IP_3Rs (IP_3-assisted CICR; Fig. 5*A*). Peak Ca^{2+} increases were 19.0 ± 2.8% (N), 51.4 ± 8.7% (S), and 106.9 ± 14.5% (D) after Cch application and did not differ significantly from those before Cch application (N, 20.7 ± 2.7%; S, 58.6 ± 8.4%; D, 122.9 ± 22.6%; $n = 5$). On the other hand, bath-application of apamin left the amplitude and time course of the slow $[Ca^{2+}]_i$ increase unchanged (Fig. 5*B*). Peak Ca^{2+} increases were 56.9 ± 3.2% (D),

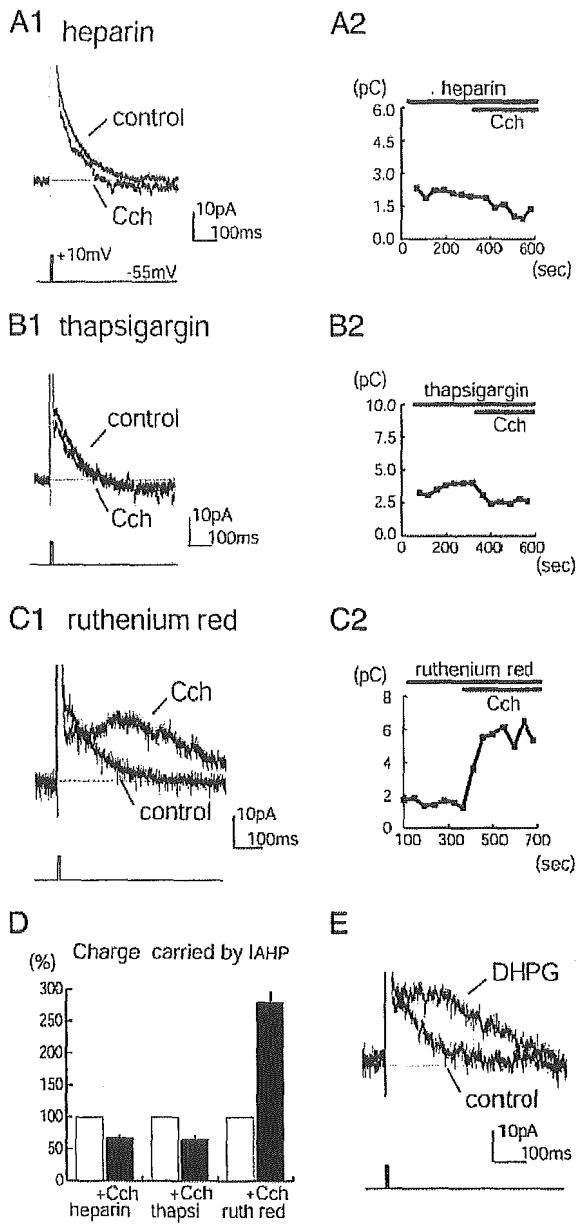

FIG. 3. Critical role played by Ca^{2+} release via inosiol-1,4,5-trisphosphate receptors (IP_3Rs) in the Cch-induced enhancement of I_{AHP}. *A1*: heparin injection prevented the Cch-induced enhancement of I_{AHP}. With heparin, Cch application rather reduced I_{AHP} (Cch). *A2*: time course of the drug effects on the charge transfer illustrated similarly to Fig. 1*B2*. *B, 1* and *2*: thapsigargin also prevented the enhancement of I_{AHP} by Cch. *C, 1* and *2*: ruthenium red left the effect of Cch unchanged. *D*: the summary diagram of the drug effects on the charge transfer. *E*: (RS)-3,5-dihydroxyphenylglycine (DHPG) enhanced I_{AHP}.

101.8 ± 11.1% (S), and 148.6 ± 9.1% (N) after Cch application and significantly greater than before Cch application (N, 16.2 ± 1.4%, $P < 0.001$; S, 55.2 ± 11.1%, $P < 0.05$; D, 93.3 ± 6.7%, $P < 0.05$; $n = 3$). Thus taken together with the findings on I_{AHP}, heparin blocked both the slow component of Ca^{2+} elevation and the slow enhancement of I_{AHP}, without affecting SK channels directly. On the other hand, apamin blocked SK channels directly and thereby abolished the slow enhancement of I_{AHP} despite occurrence of the slow phase of $[Ca^{2+}]_i$ increase. We therefore concluded that the slow Ca^{2+} elevation, which represents IP_3-assisted CICR (Yamamoto et al. 2000), activates apamin-sensitive SK channels.

Cch-induced enhancement of spike-frequency adaptation depended on SK channels

As shown thus far, IP_3R activation added a second slow phase of depolarization-induced SK currents to the first phase, which was evoked already without IP_3R activation. The entire time course of SK currents was thereby prolonged, and the total outward charge transfer increased. We then tested whether such prolongation of SK currents really decreases membrane excitability after spike discharge. Under current clamp, Cch deepened and prolonged mAHP induced by a single action potential (Fig. 6*A*). The amplitude of mAHP was 4.46 ± 0.55 mV without Cch and became significantly larger with Cch (6.16 ± 0.52 mV; $n = 5$, $P < 0.05$; Fig. 6*C*). The time to peak of mAHP was also significantly longer with Cch (228 ± 15 ms) than without Cch (149 ± 10 ms, $n = 5$, $P < 0.01$). Intracellular injection of heparin curtailed this effect of Cch. With heparin intracellularly injected, the mAHP amplitude (2.18 ± 0.24 mV before Cch application) was not enlarged by Cch application (0.92 ± 0.3 mV, $n = 5$; Fig. 6*B*). Rather the mAHP amplitude was reduced, and a presumed spike afterdepolarization was overridden. Spike-induced calcium release from IP_3Rs (IP_3-assisted CICR) was thus suggested to play a critical part in the Cch-induced enlargement of mAHP.

Furthermore, calcium imaging revealed that the Cch-induced enhancement of mAHP during single spikes was accompanied by increases in spike-induced calcium elevation. We plotted Ca^{2+} increase during a single spike in a ROI located at the soma-dendrite border (Fig. 6*D*). After application of Cch, a delayed phase of calcium elevation emerged, and the whole calcium increase was enhanced (red line, Fig 6*D*). According to the findings obtained with voltage clamp (Fig. 4), the enhanced part of Ca^{2+} increase is likely to represent spike-induced calcium release. The peak calcium increase after Cch application, expressed by percent of the control level ($\Delta F/F$), was significantly greater (74.2 ± 13.7%) than before Cch application (41.2 ± 4.1%, $P < 0.05$; $n = 4$). Thus spike-induced calcium release from IP_3Rs was suggested to contribute to Cch-induced enhancement of mAHP during a single spike.

We then examined effects of Cch on repetitive spike firing. Depolarizing currents of longer duration (500 ms) were injected. On injection, all the neurons fired in the regular spiking fashion (McCormick et al. 1985). The current intensity was adjusted to evoke 8–10 action potentials for 500 ms. Cch application enhanced spike-frequency adaptation as previously reported (Yamamoto et al. 2002a) and diminished the number of action potentials by 1.6 ± 0.3 ($n = 9$, $P < 0.01$; Fig. 7*A* and *B*). Then by using the SK channel blocker apamin, it was studied whether this Cch-induced enhancement of spike-frequency adaptation depends on SK channels. Currents of the same intensity evoked a larger number of spikes (9.7 ± 0.62) in apamin-containing medium than in control medium (7.7 ±

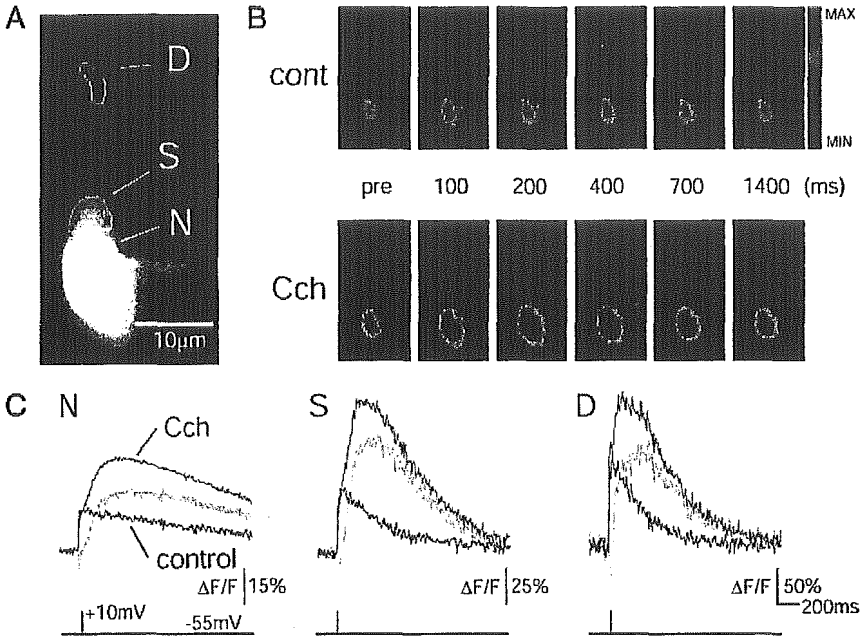

FIG. 4. Slow enhancement of depolarization-induced $[Ca^{2+}]_i$ increase by Cch. *A*: fluorescence image of a pyramidal cell. To calculate the time course of Ca^{2+} concentration changes, regions of interest (ROIs) were selected over the nucleus (N), extranuclear soma (S), and proximal dendrite (D). *B* and *C*: $[Ca^{2+}]_i$ increase without (black lines) and with Cch (red lines). The green lines in *C*, as well as those in Fig. 5, indicate the subtractions between black and red lines; hence the net enhancement of $[Ca^{2+}]_i$ increase.

0.62, $P < 0.03$, $n = 10$). Therefore the current intensity under apamin application was so reduced that much the same numbers of spikes could be evoked as in normal medium. To confirm the dependence of Cch-induced effects on SK channels, we first recorded spike firing under blockade of SK channels by apamin, and then Cch was further applied. Under SK channel blockade by apamin, Cch application failed to enhance spike-frequency adaptation, confirming our conclusion that Cch-induced enhancement of spike-frequency adaptation depends on SK channels. Cch application rather increased the number of action potentials by 1.8 ± 0.5 ($n = 10$, $P < 0.001$). This excitability increase is due likely to blockade of M channels by Cch (Marrion 1997) because the M channel blocker linopirdine slightly exaggerated the Cch-induced enhancement of spike-frequency adaptation ($n = 8$, data not shown). The BK channel blocker iberiotoxin failed to affect Cch-induced enhancement of spike-frequency adaptation ($n = 7$, data not shown), again supporting the conclusion that SK channels are the target of depolarization-induced calcium release enabled by mAchR activation.

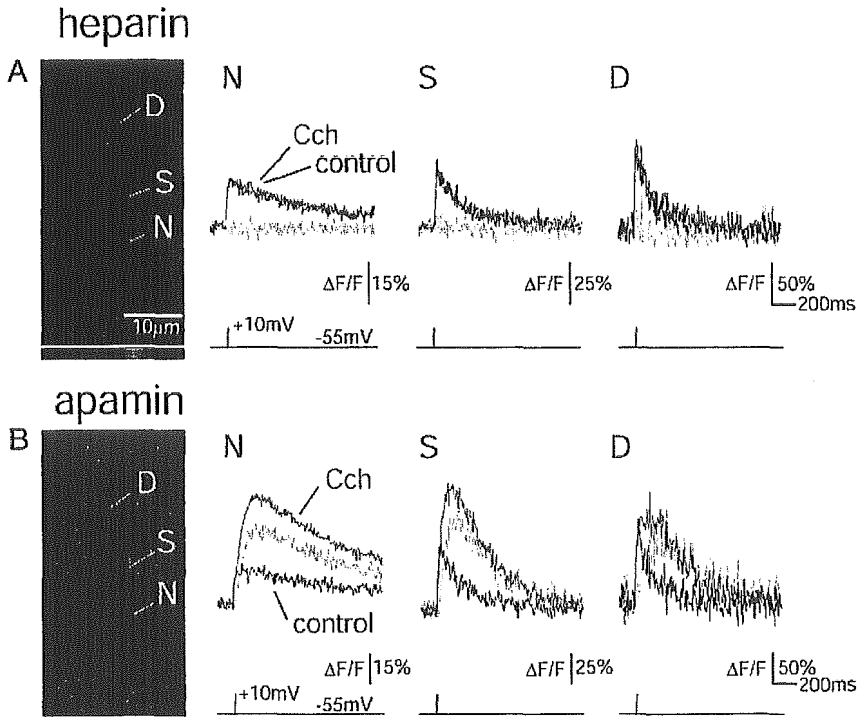

FIG. 5. Pharmacological perturbation of the Cch-dependent, slow enhancement of depolarization-induced $[Ca^{2+}]_i$ increase. *A*: heparin prevented the enhancement of $[Ca^{2+}]_i$ increase by Cch. *B*: bath-application of apamin left the amplitude and time course of the slow $[Ca^{2+}]_i$ increase unchanged.

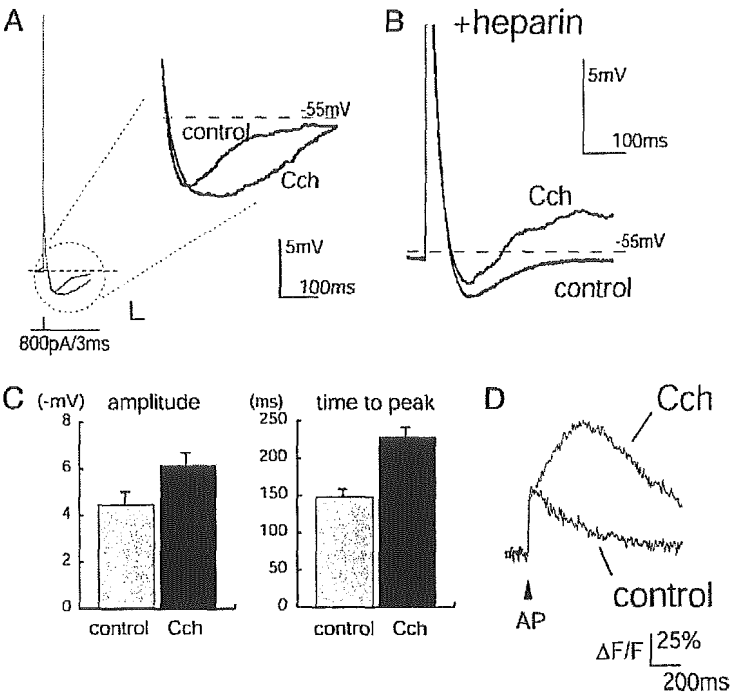

FIG. 6. Cch-induced enhancement of medium afterhyperpolarization (mAHP) and spike-induced calcium release after a single action potential. *A*: Cch deepened and prolonged mAHP after a single action potential. Single spikes were induced by injecting depolarizing currents. Intensity and duration of the current were adjusted to induce a single action potential. *B*: intracellular application of heparin blocked the effect of Cch on mAHP, suggesting that the Cch effect depends on IP3Rs. *C*: the depth (amplitude) and time to peak were both significantly larger with Cch than without, which clearly indicates an enhancement of mAHP rather than fast AHP (fAHP). Heparin prevented these effects of Cch. *D*: $[Ca^{2+}]_i$ increase with (red line) and without Cch (black line) during a single spike, obtained from a ROI located at the soma-dendrite border (see Fig. 4). Cch application enhanced calcium increase induced by a single spike. The net enhancement of $[Ca^{2+}]_i$ increase exhibited a delayed time course similar to that obtained by using voltage clamp (Fig. 4), suggesting that the enhanced part is due to calcium release.

DISCUSSION

The present experiments demonstrated a Ca^{2+}-dependent, functional triad composed of VDCCs, IP_3Rs, and SK channels. This triad is linked functionally by spike-triggered Ca^{2+} inflow and Ca^{2+} release from IP_3Rs. Although it remains unknown whether these channels are physically coupled or not, we have at least revealed a functional linkage among them. This functional triad regulates spike-frequency adaptation under the influence of IP_3-mobilizing neurotransmitters. Spike-frequency adaptation may operate even with this triad switched off, depending solely on VDCCs and SK channels. Our discussion in the following text is focused on how functionally advantageous the mode of spike-frequency adaptation could become once this triad is switched on.

Spike-frequency adaptation is a typical example of Ca^{2+}-mediated regulation of membrane excitability in which a class of Ca^{2+}-activated K^+ channels, SK channels, are activated by spike-induced increases in intracellular Ca^{2+}, thereby stabilizing membrane excitability in a negative feedback fashion (Sah 1996). SK channels, activated voltage-independently and inactivated with a slow time course (Hirschberg et al. 1998), play the principle role in spike-frequency adaptation by evoking mAHP (Sah 1996). Because spike firing opens VDCCs and generate mAHP, it is naturally understood that Ca^{2+} entry through VDCCs will attenuate spike firing in a feedback manner (Sah and Davies 2000). The gain of this minimal feedback may not necessarily depend on the firing rate because the *per spike* Ca^{2+} increase here has been shown constant (Yamamoto et al. 2002a). As a second source of Ca^{2+} increase, IP_3-induced Ca^{2+} released from IP_3Rs (IICR) is also reported to open Ca^{2+}-activated K^+ channels including SK channels in midbrain (Fiorillo and Williams 1998, 2000; Morikawa et al. 2000) and neocortex neurons (Stutzmann et al. 2003). However, because IICR occurs depending on release of neurotransmitters that lead to IP_3 synthesis but not on spike firing, a direct activation of SK channels by IICR cannot constitute a feedback

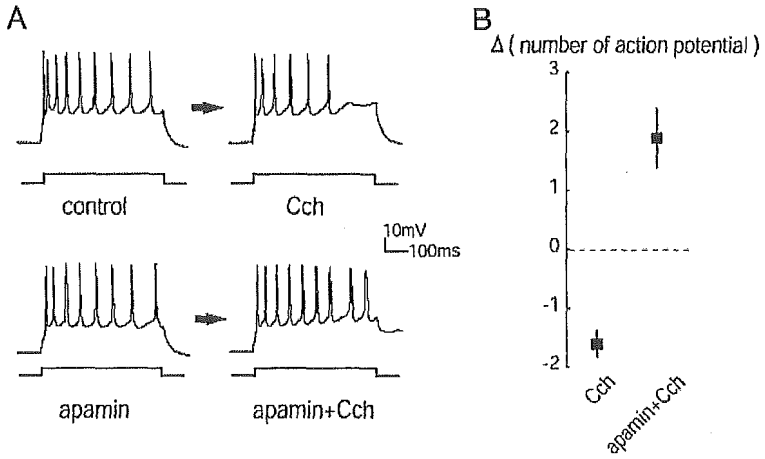

FIG. 7. Enhancement of spike-frequency adaptation by Cch application depends on small conductance Ca^{2+} dependent K^+ (SK) channels. In control medium, Cch diminished the number of action potentials induced by a 500-ms-long depolarization pulse (*A*, *top*; *B*, Cch). Under blockade of SK channels by apamin, Cch application rather increased their number (*A*, *bottom*; *B*, apamin + Cch). Note that apamin application makes firing rate higher than in control medium when currents of the same intensity was injected. Therefore before Cch application, the current intensity in apamin-containing medium was so adjusted that much the same numbers of spikes could be evoked as in normal medium.

regulation of spike firing. Also, an upregulation of SK channels by IICR would not slow down the time course of Ca^{2+} entry and therefore would not explain the associated emergence of the slow components of both Ca^{2+} increase and I_{AHP} shown in the present experiments. As a third possibility, spike-triggered Ca^{2+} influx persuades RyRs to release Ca^{2+} [the conventional CICR (Llano et al. 1994; Verkratsky and Shmigol 1996)], which was documented to open Ca^{2+}-activated K^+ channels, including SK channels, in sympathetic neurons (Akita and Kuba 2000; Davies et al. 1996; Jobling et al. 1993). This conventional CICR could therefore boost the ability of spike-triggered Ca^{2+} influx to open SK channels activity-dependently. Some intracellular signals, such as cADP ribose or FK binding protein, are known to modulate RyRs in neurons (Berridge 1998; Higashida et al. 2001). However, these signals are not unequivocally shown to be mobilized by extracellular signals like neurotransmitters. Thus so far, a synaptic control cannot be held possible on spike firing regulation based on the conventional CICR.

Yet another form of CICR has been described in hippocampus (Nakamura et al. 1999; Power and Sah 2002) and neocortex pyramidal cells (Larkum et al. 2003; Yamamoto et al. 2000). Here, IP_3Rs are initially primed by IP_3 increase, and then a subsequent spike-induced inflow of Ca^{2+} triggers Ca^{2+} release from IP_3Rs. This is a CICR by definition. But, Ca^{2+} is released from IP3Rs instead of RyRs. Also, this mode of CICR, called IP_3-assisted CICR in Yamamoto et al. (2000, 2002a), is different from IICR that is triggered by increase in IP_3 alone. The functional significance of IP_3-assisted CICR seems to originate from the supra-linearity of the *per spike* Ca^{2+} increase during its occurrence (Yamamoto et al. 2002a). The present findings have shown that Ca^{2+} recruited by IP_3-assisted CICR aimed at SK channels in pyramidal cells. A functional triad is thus established that consists of VDCCs, IP_3Rs, and SK channels. With this triad, because of an activity-dependent Ca^{2+} release, the *per spike* Ca^{2+} increase may grow supra-linearly with the firing rate increased, resulting in a supra-linear increase in SK channel open probability. Thus the gain of spike-frequency adaptation will be modified activity-dependently. Such gain modifiability may enable a finer tuning of spike firing. More remarkably, this gain control is regulated synaptically by neurotransmitters leading to IP_3 synthesis.

ACKNOWLEDGMENTS

The authors thank Dr. Kenji Yamamoto for helpful advice.

GRANTS

This work was supported by Grants-in-Aid for Scientific Research and Center of Excellence Grant 12CE2006 from the Ministry of Education, Culture, Sports, Science and Technology of Japan.

REFERENCES

Akita T and Kuba K. Functional triads consisting of ryanodine receptors, Ca^{2+} channels, and Ca^{2+}-activated K^+ channels in bullfrog sympathetic neurons. Plastic modulation of action potential. *J Gen Physiol* 116: 697–720, 2000.

Berridge MJ. Neuronal calcium signaling. *Neuron* 21: 13–26, 1998.

Bezprozvanny I, Watras J, and Ehrlich BE. Bell-shaped calcium response curves of Ins(1,4,5)P_3-and calcium gated channels from endoplasmic reticulum of cerebellum. *Nature* 351: 751–754, 1991.

Choi DW. Calcium: still center-stage in hypoxic-ischemic neural death. *Trends Neurosci* 18: 58–60, 1985.

Davies PJ, Ireland DR, and McLachlan EM. Sources of Ca^{2+} for Ca^{2+}-activated K^+ conductance in neurons of the rat superior cervical ganglion. *J Physiol* 495: 353–366, 1996.

Emptage N, Bliss TV, and Fine A. Single synaptic events evoke NMDA receptor-mediated release of calcium from internal stores in hippocampal dendritic spines. *Neuron* 22: 115–124, 1999.

Finch EA, Turner TJ, and Goldin SM. Calcium as a coagonist of inositol 1,4,5-triphosphate-induced calcium release. *Science* 252: 443–446, 1991.

Fiorillo CD and Williams JT. Glutamate mediates an inhibitory postsynaptic potential in dopamine neurons. *Nature* 394: 78–82, 1998.

Fiorillo CD and Williams JT. Cholinergic inhibition of ventral midbrain dopamine neurons. *J Neurosci* 20: 7855–7860, 2000.

Higashida H, Hashii M, Yokoyama S, Hoshi N, Asai K, and Kato T. Cyclic ADP-ribose as a potential second messenger for neuronal Ca^{2+} signaling. *J Neurochem* 76: 321–331, 2001.

Hirschberg B, Maylie J, Adelman JP, and Marrion NV. Gating of recombinant small-conductance Ca-activated K^+ channels by calcium. *J Gen Physiol* 111: 565–581, 1998.

Iino M. Biphasic Ca^{2+} dependence of inositol 1,4,5-triphosphate-induced Ca release in smooth muscle cells of guinea pig taenia caeci. *J Gen Physiol* 95: 1103–1122, 1990.

Isaacson JS and Murphy GJ. Glutamate-mediated extrasynaptic inhibition: direct coupling of NMDA receptors to Ca^{2+} activated K^+ channels. *Neuron* 31: 1027–1034, 2001.

Jobling P, McLachlan EM, and Sah P. Calcium induced calcium release is involved in the afterhyperpolarization in one class of guinea pig sympathetic neuron. *J Auton Nerve Syst* 42: 251–257, 1993.

Larkum ME, Watanabe S, Nakamura T, Lasser-Ross N, and Ross WN. Synaptically activated Ca^{2+} waves in layer 2/3 and layer 5 rat neocortical pyramidal neurons. *J Physiol* 549: 471–488, 2003.

Llano I, DiPolo R, and Marty A. Calcium-induced calcium release in cerebellar Purkinje cells. *Neuron* 12: 663–673, 1994.

Lynch G, Larson J, Kelso S, Barrionuevo G, and Schottler F. Intracellular injections of EGTA block induction of hippocampal long-term potentiation. *Nature* 305: 719–721, 1983.

Marrion NV. Control of M-current. *Annu Rev Physiol* 59: 483–504, 1997.

McCormick DA, Connors BW, Lighthall JW, and Prince DA. Comparative electrophysiology of pyramidal and sparsely spiny stellate neurons of the neocortex. *J Neurophysiol* 54: 782–806, 1985.

McCormick DA and Contreras D. On the cellular and network bases of epileptic seizures. *Annu Rev Physiol* 63: 815–846, 2001.

Morikawa H, Imani F, Khodakhah K, and Williams JT. Inositol 1,4,5-trsiphosphate-evoked responses in midbrain dopamine neurons. *J Neurosci* 20: 1–5, 2000.

Nakamura T, Barbara JG, Nakamura K, and Ross WN. Synergistic release of Ca^{2+} from IP_3-sensitive stores evoked by synaptic activation of mGluRs paired with backpropagating action potentials. *Neuron* 24: 727–737, 1999.

Nakamura T, Nakamura K, Lasser-Ross N, Barbara JG, Sandler VM, and Ross WN. Inositol 1,4,5-triphosphate (IP_3)-mediated Ca^{2+} release evoked by metabotropic agonists and backpropagating action potentials in hippocampal CA1 pyramidal neurons. *J Neurosci* 20: 8365–8376, 2000.

Partridge LD and Valenzuela CF. Ca^{2+} store-dependent potentiation of Ca^{2+}-activated non-selective cation channels in rat hippocampal neurones in vitro. *J Physiol* 521: 617–627, 1999.

Power JM and Sah P. Nuclear calcium signaling evoked by cholinergic stimulation in hippocampal CA1 pyramidal neurons. *J Neurosci* 22: 3454–3462, 2002.

Randall AD. The molecular basis of voltage-gated Ca^{2+} channel diversity: Is it time for T? *J Membr Biol* 161: 207–213, 1998.

Rose CR and Konnerth A. Stores not just for storage: intracellular calcium release and synaptic plasticity. *Neuron* 31: 519–522, 2001.

Sah P. Ca^{2+}-activated K^+ currents in neurones: types, physiological roles and modulation. *Trends Neurosci.* 19: 150–154, 1996.

Sah P and Davies P. Calcium-activated potassium currents in mammalian neurons. *Clin Exp Pharmacol Physiol* 27: 657–663, 2000.

Sakurai M. Calcium is an intracellular mediator of the climbing fiber in induction of cerebellar long-term depression. *Proc Natl Acad Sci USA* 87: 3383–3385, 1990.

Stutzmann GE, LaFerla FM, and Parker M. Ca^{2+} signaling in mouse cortical neurons studied by two-photon imaging and photoreleased inositol trsiphosphate. *J Neurosci* 23: 758–765, 2003.

Verkratsky A and Shmigol A. Calcium-induced calcium release in neurones. *Cell Calcium* 19: 1–14, 1996.

Wang SS, Denk W, and Hausser M. Coincidence detection in single dendritic spines mediated by calcium release. *Nat Neurosci* 3: 1266–1273, 2000.

Yamamoto K, Hashimoto K, Isomura, Y, Shimohama S, and Kato N. An IP_3-assisted form of Ca^{2+}-induced Ca^{2+} release in neocortical neurons. *Neuroreport* 11: 535–539, 2000.

Yamamoto K, Hashimoto K, Nakano M, Shimohama S, and Kato N. A distinct form of calcium release down-regulates membrane excitability in neocortical pyramidal cells. *Neuroscience* 109: 665–676, 2002a.

Yamamoto K, Nakano M, Hashimoto K, Shimohama S, and Kato N. Emergence of a functional coupling between inositol-1,4,5-triphosphate receptors and calcium channels in developing neocortical neurons. *Neuroscience* 109: 677–685, 2002b.

Yang J, McBride S, Mak DD, Vardi N, Palczewski K, Haeseleer F, and Foskett JK. Identification of a family of calcium sensors as protein ligands of inositol trisphosphate receptor Ca^{2+} release channels. *Proc Natl Acad Sci USA* 99: 7711–7716, 2002.

Targeted Disruption of TGF-β–Smad3 Signaling Leads to Enhanced Neointimal Hyperplasia With Diminished Matrix Deposition in Response to Vascular Injury

Kazuki Kobayashi, Koutaro Yokote, Masaki Fujimoto, Kimihiro Yamashita, Akemi Sakamoto, Masaki Kitahara, Harukiyo Kawamura, Yoshiro Maezawa, Sunao Asaumi, Takeshi Tokuhisa, Seijiro Mori, Yasushi Saito

Abstract—The role of transforming growth factor (TGF)-β and its signal in atherogenesis is not fully understood. Here, we examined mice lacking Smad3, a major downstream mediator of TGF-β, to clarify the precise role of Smad3-dependent signaling in vascular response to injury. Femoral arteries were injured in wild-type and Smad3-null (null) male mice on C57Bl/6 background. Histopathological evaluation of the arteries 1 to 3 weeks after the injury revealed significant enhancement of neointimal hyperplasia in null compared with wild-type mice. Transplantation of null bone marrow to wild-type mice did not enhance neointimal thickening, suggesting that vascular cells in situ play a major role in the response. Null intima contained more proliferating smooth muscle cells (SMC) with less amount of collagen compared with wild-type intima. TGF-β caused significant inhibition of cellular proliferation in wild-type aortic SMC, whereas the growth of null SMC was only weakly inhibited by TGF-β in vitro, indicating a crucial role of Smad3 in the growth inhibitory function. On the other hand, Smad3-deficiency did not attenuate chemotaxis of SMC toward TGF-β. TGF-β increased transcript level of α2 type I collagen and tissue inhibitor of metalloproteinases-1, and suppressed expression and activity of matrix metalloproteinases in wild-type SMC. However, these effects of TGF-β were diminished in null SMC. Our findings altogether show that the loss of Smad3 pathway causes enhanced neointimal hyperplasia on injury through modulation of growth and matrix regulation in vascular SMC. These results indicate a vasculoprotective role of endogenous Smad3 in response to injury. (*Circ Res.* 2005;96:000-000.)

Key Words: transforming growth factor-β ■ Smad3 ■ atherosclerosis ■ neointimal hyperplasia ■ smooth muscle cells

Transforming growth factor (TGF)-β is a prototypic member of the TGF-β superfamily that exerts a wide range of biological effects on various cell types.[1] Well described functions of TGF-β including growth inhibition, cell migration, differentiation, extracellular matrix production, and immunomodulation. Abnormality in TGF-β signaling may cause pathological conditions such as tumorigenesis, fibrotic disorders, and vascular diseases.[2] At present, however, the role of TGF-β and its signaling molecules in atherogenesis is not fully understood.

TGF-β is often regarded to have proatherosclerotic effect on arteries. For example, TGF-β expression is increased in human restenotic lesions as well as in neointimal hyperplasia after balloon injury in animals.[3] TGF-β facilitates extracellular matrix deposition by stimulating production of procollagen and fibronectin, downregulating the expression of proteases, and upregulating protease inhibitors, such as plasminogen activator inhibitor type I (PAI-I) and tissue inhibitor of metalloproteinase-1 (TIMP-1).[4–8] TGF-β transgene into vascular wall causes fibroproliferative intimal thickening in animal models in the presence or absence of vascular injury.[9,10] Moreover, TGF-β antagonism by antibody, soluble receptor, or ribozyme reduces constrictive remodeling after balloon injury in animals.[11–13]

On the other hand, considerable evidence implies antiatherosclerotic effects of TGF-β. TGF-β has been shown to inhibit proliferation and migration of vascular smooth muscle cells (SMCs) in vitro.[14,15] Inhibition of TGF-β signal systemically by use of neutralizing antibody and soluble TGF-β receptor type (TβR)-II or in T-cells by expressing a dominant-negative TβR-II results in an unstable plaque phenotype in mouse models of atherosclerosis.[16–18] SMCs

Original received September 13, 2004; resubmission received February 9, 2005; revised resubmission received March 14, 2005; accepted March 17, 2005.

From the Department of Clinical Cell Biology (K.K., K.Y., M.F., H.K., Y.M., S.A., S.M., Y.S.), Chiba University Graduate School of Medicine; Division of Endocrinology and Metabolism (K.Y., Y.S.), Department of Internal Medicine, Chiba University Hospital; Department of Developmental Genetics (K.Y., A.S., T.T.), Chiba University Graduate School of Medicine, Chiba, Japan; and Shiraoka Research Station of Biological Science (M.K.), Nissan Chemical Industries, Ltd, Saitama, Japan.

Correspondence to Koutaro Yokote, MD, PhD, DMSci, Division of Endocrinology and Metabolism, Department of Internal Medicine, Chiba University Hospital, 1-8-1 Inohana, Chuo-ku, Chiba 260-8670, Japan. E-mail kyokote-cib@umin.ac.jp

Circulation Research is available at http://www.circresaha.org

DOI: 10.1161/01.RES.0000163980.55495.44

obtained from human atherosclerotic plaques were shown to be defective in the TGF-β signal pathway and were resistant to TGF-β–mediated growth suppression and apoptosis.[19,20] Furthermore, low blood levels of active TGF-β were associated with severity of vascular disease in a manner consistent with an antiatherosclerotic effect of TGF-β.[21]

TGF-β elicits its effects via signaling through tetramerization of two different receptor serine/threonine kinases, TβR-I and TβR-II.[22,23] Activation of the receptors leads to phosphorylation of cytoplasmic signal transducers Smad2 and Smad3, classified as so-called receptor-activated Smads (R-Smad). The activated R-Smad heteroligomerizes with Smad4, a common mediator Smad, and the complex is transported to the nucleus where it regulates gene expression. In addition, pathways independent of Smads, which involve MAP kinases have also been described.[23] In mice lacking TGF-β signaling molecules, ie, TβR-I and TβR-II, Smad2 and Smad4 turned out to be embryonic lethal.[24–26] However, it was recently found that the mice null for Smad3 survive into adulthood.[27]

We undertook the present study examining Smad3-null mice in vivo and in vitro to elucidate the precise role of Smad3-dependent TGF-β signaling in the vascular response to injury.

Materials and Methods

Reagents

Reagents are described in an expanded Materials and Methods section in the online data supplement available at http://circres.ahajournals.org.

Mice

The generation of $Smad3^{ex8/ex8}$ null mice by homologous recombination was described previously.[27] See expanded Materials and Methods section for details.

Femoral Artery Injury

Mice femoral arteries were injured by use of photochemically-induced thrombosis method.[28] See expanded Materials and Methods section for details.

Histological Evaluation

Fixed femoral artery segments were embedded in paraffin and cut into 5-μm–thick serial sections. Six sections per one irradiated segment at 1-mm intervals were stained with hematoxylin and eosin. Neointima was defined as the region between the lumen and the internal elastic lamina. The media was defined as the region between the internal and external elastic lamina. The cross-sectional areas of intima and media were measured using *NIH image version 1.62f* (National Institutes of Health, USA). The intima-to-media (I/M) ratio was then calculated, and the mean I/M of all 6 sections per one irradiated segments was determined. The sections with intimal hyperplasia were also subjected to Masson's trichrome staining and immunohistochemistry. Masson's trichrome-positive intimal area was analyzed using Photoshop version 7.0 (Adobe). All the measurements were made in blinded manner.

Immunohistochemistry

Immunohistochemistry is described in the expanded Materials and Methods section.

Bone Marrow Transplantation

Bone marrow transplantation (BMT) was performed principally as described previously.[29] Briefly, bone marrow cell suspensions obtained from either Smad3-null or wild-type mice thigh bone were treated with ACK lysis buffer (0.155 mol/L ammonium chloride, 0.1 mol/L disodium EDTA, and 0.01 mol/L potassium bicarbonate) to lyse erythrocytes. The cells were intravenously injected to recipient Smad3-null or wild-type mice (1×10^6 per body) between the age of 6 and 9 weeks 3 hours after lethal irradiation (8.5 Gy). Engraftment of the transferred bone marrow was confirmed by polymerase chain reaction (PCR) on peripheral blood DNA according to the protocol by Yang et al.[26] Femoral artery injury was performed 6 weeks after the bone marrow transfer.

Cell Culture

Mouse aortic SMCs were obtained and cultured as described by Ohmi et al[30] (see expanded Materials and Methods section). Experiments were performed on cells after 5 to 10 passages from the primary culture.

Immunocytochemistry

Immunocytochemical staining using anti–α-SMA and SMM antibodies was performed as described by Hasegawa et al[31] with some modification (see expanded Materials and Methods section).

Immunoblotting

Immunoblotting was essentially performed as previously described[32] (see expanded Materials and Methods section).

Growth Inhibition Assay

Growth inhibition assay was performed as described by Datto et al[33] (see expanded Materials and Methods section).

Cell Migration Assay

SMC migration was evaluated by modified Boyden chamber method[34] (see expanded Materials and Methods section).

Real-Time Quantitative PCR

Real-time quantitative PCR is described in expanded Materials and Methods section.

Gelatin Zymography

Gelatin zymography is described in the expanded Materials and Methods section.

Statistical Analysis

Results were presented as mean±SEM. Statistical analyses used two-tailed, unpaired student *t* test.

Results

Mice Lacking Smad3 Show Enhanced Neontimal Hyperplasia in Response to Injury

To evaluate a role of Smad3 in the pathogenesis of neointimal hyperplasia, femoral arteries of wild-type (n=12) and Smad3-null (n=10) male mice were injured by use of photochemically-induced thrombosis method.[26] Histopathological examination of the arteries 1 to 3 weeks after the injury revealed markedly enhanced neointimal thickening in Smad3-null mice compared with wild-type mice (Figure 1A and 1B). As shown in Figure 1C, mean I/M ratios evaluated at 1 and 3 weeks after the injury were significantly higher in Smad3-null arteries (0.193±0.034 at 1 week and 0.541±0.093 at 3 weeks) than those of wild-type arteries (0.059±0.018 at 1 week and 0.115±0.060 at 3 weeks, $P<0.01$ at each time point).

Immunohistochemical examination showed that both neointimal and medial cells were positive for α-SMA (Figure 2A and 2B) but negative for pan-leukocyte marker CD45 (Figure

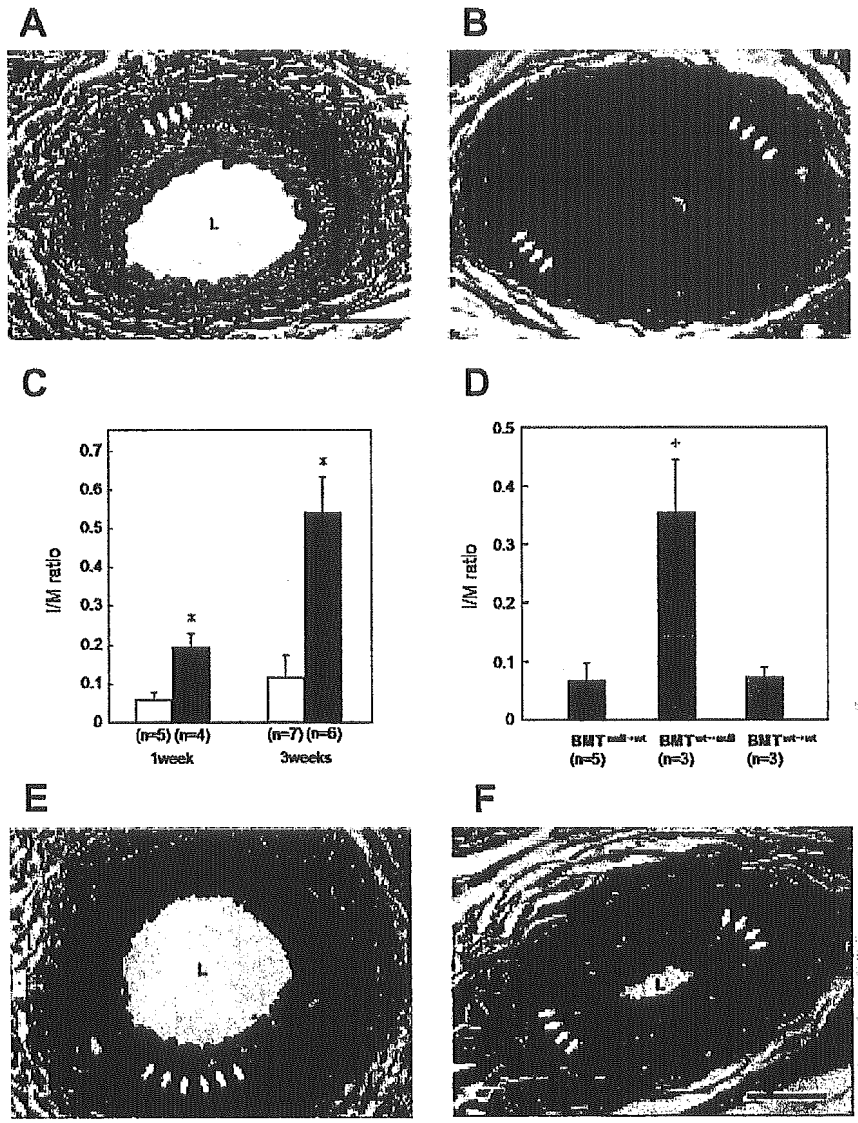

Figure 1. Neointimal thickening in injured femoral arteries of wild-type and Smad3-null mice. Photomicrographs showing representative cross sections of hematoxylin and eosin–stained femoral arteries from wild-type (A) and Smad3-null (B) and $BMT^{null\rightarrow wild}$ (E) and $BMT^{wild\rightarrow null}$ (F) mice 3 weeks after endothelial injury. L indicates vascular lumen. Arrows indicate the positions of the internal elastic lamina. Original magnification ×200; bar=50 μm. Intima-to-media (I/M) ratios at 1 and 3 weeks in wild-type and Smad3-null mice (C) and in $BMT^{null\rightarrow wild}$, $BMT^{wild\rightarrow null}$, and $BMT^{wild\rightarrow wild}$ at 3 weeks (D) were calculated from cross sectional areas morphometrically measured using an image analyzer. Open and closed columns indicate wild-type and Smad3-null mice, respectively. *$P<0.01$ compared with wild type at each time point; †$P<0.05$ compared with $BMT^{null\rightarrow wild}$.

2C and 2D), indicating that the intima was exclusively composed of SMCs. The same anti-CD45 antibody recognized leukocytes in vasa vasorum (Figure 2D) as well as lymphocytes in the mouse spleen (Figure 2E).

TGF-β is well known for its antiinflammatory effect.[1,2] To determine whether systemic inflammation due to Smad3 deficiency contributes to enhanced neointimal formation, we injured femoral artery of wild-type and Smad3-null mice after bone marrow transplantation (BMT). Lethally irradiated Smad3-null mice received 1×10^6 bone marrow cells from a wild-type mouse ($BMT^{wild\rightarrow null}$ mice). At the same time, irradiated wild-type mice were given bone marrow either from Smad3-null or wild-type mice ($BMT^{null\rightarrow wild}$ and $BMT^{wild\rightarrow wild}$ mice). Photochemical injury was performed 6 weeks after the bone marrow transfer, and the arterial cross section was analyzed 3 weeks later. As shown in Figure 1D, mean I/M ratio was significantly higher in $BMT^{wild\rightarrow null}$ arteries (0.353 ± 0.091) than those of $BMT^{null\rightarrow wild}$ (0.067 ± 0.031, $P=0.011$) or $BMT^{wild\rightarrow wild}$ (0.073 ± 0.018, $P=0.039$) arteries. I/M ratios in $BMT^{wild\rightarrow null}$ and $BMT^{null\rightarrow wild}$ mice tended to be lower than those of Smad3-null and wild-type mice, respectively, presumably due to the effect of vascular irradiation.[35,36] Representative cross sections of $BMT^{null\rightarrow wild}$ and $BMT^{wild\rightarrow null}$ femoral arteries are shown in Figure 1E and 1F.

Smad3-Null Intima Is Rich in Proliferating Cells but Contains Low Amounts of Collagen Fibers

Intimal cell proliferation was assessed by immunohistochemical detection of PCNA in the femoral artery sections 1 week after the injury (Figure 3A and 3B). The ratio of the PCNA-positive nuclei to total cell nuclei was higher by 1.8-fold in Smad3-null intima compared with wild-type intima (Figure 3C). The result shows an increased proliferative activity of SMCs in Smad3-null artery at the early stage after injury.

We next evaluated intimal cell density in hematoxylin and eosin–stained arterial sections 3 weeks after the injury. As shown in Figure 4A, the ratio of intimal cell number to total intimal area was 1.6-fold higher in Smad3-null artery

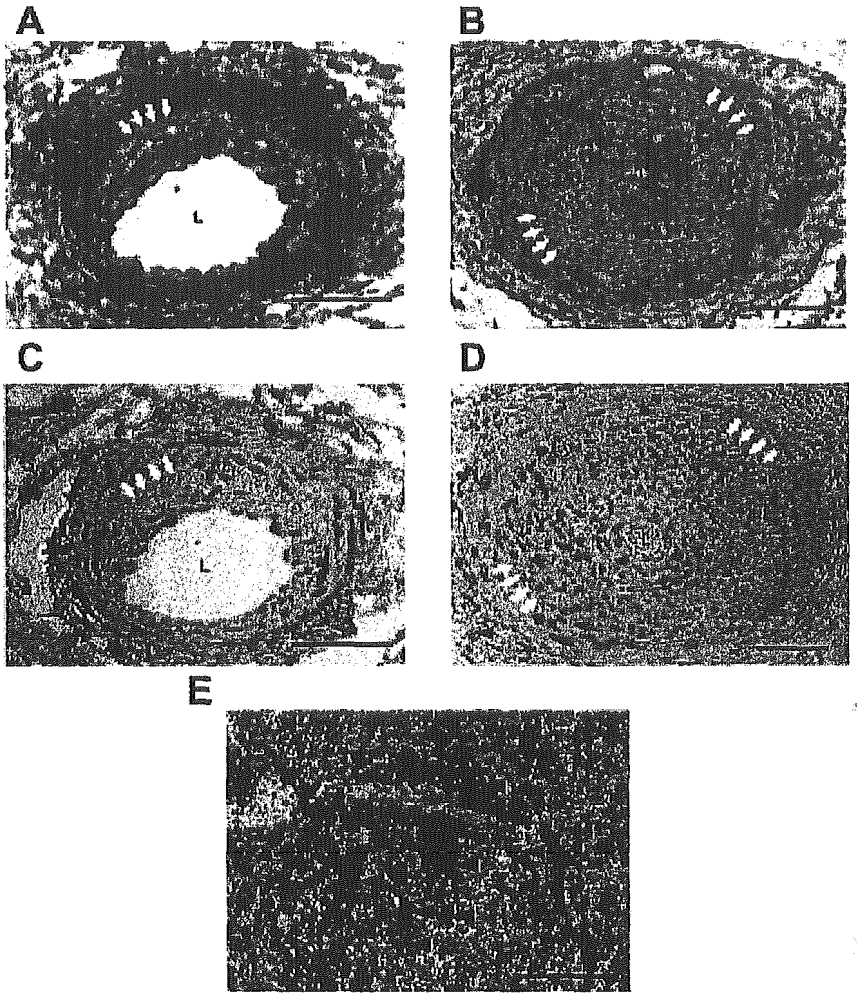

Figure 2. Immunohistochemical analysis of neointimal components. Cross sections of femoral arteries from wild-type (A and C) and Smad3-null (B and D) mice 3 weeks after endothelial injury and of mouse spleen (E). Immunostaining was performed using specific antibodies for α-SMA (A and B) and CD45 (C, D, and E). L indicates vascular lumen. Arrows indicate the positions of the internal elastic lamina. Arrowheads indicate the positions of representative CD45-positive leukocytes. Original magnification ×200; bar=50 μm.

(133±8.6) compared with wild-type artery (85.3±7.7, $P<0.01$), indicating higher cell density relative to extracellular area in Smad3-null intima. Because TGF-β/Smad3 signal is implicated in extracellular matrix (ECM) deposition, Masson trichrome staining was also performed on a 3-week artery specimen to evaluate the amount of extracellular collagen fibers (Figure 4C and 4D). As summarized in Figure 4B, Smad3-null neointima showed 60% reduction in the ratio of Masson trichrome-positive area to total intimal area compared with that of wild-type intima. These results suggest that Smad3 deficiency caused increased SMC number with less collagen deposition in neointima.

Growth Inhibition by TGF-β Is Attenuated in SMCs Lacking Smad3

To identify the mechanisms by which Smad3 deficiency caused exaggerated intimal hyperplasia, biological responses of the aortic SMCs obtained from wild-type and Smad3-null mice were examined in vitro. The cells were positive for both α-SMA and SMM (Figure 5A and 5B) as examined by immunocytochemistry. They also exhibited the classic "hills and valley" appearance, a feature characteristic of confluent cultured vascular SMCs. No morophological differences were observed between wild-type and Smad3-null SMCs (data not shown). It was confirmed by immunoblotting that SMCs derived from Smad3-null mice lacked expression of Smad3, whereas Smad2 level was similar in both cells (Figure 5C).

The SMCs were first tested for proliferation. As shown in Figure 6A, TGF-β dose-dependently inhibited FBS-stimulated DNA synthesis in wild-type SMCs with the maximal inhibition of 70% at 1 ng/mL and higher doses. In contrast, growth of Smad3-null SMCs was only weakly (<30%) inhibited by TGF-β. In addition, the basal growth rate of the null cells was approximately 1.4-fold higher than that of the wild-type. Similar results were obtained for two additional cell lines of each genotype. The results firmly establish an essential role for Smad3 in TGF-β–mediated inhibition of cellular proliferation in vascular SMCs.

Smad3 Deficiency Does Not Attenuate TGF-β–Mediated Migratory Response in SMCs

The cells were next examined for migration, another function crucial to neointimal formation. Aschcroft et al[37] previously reported that Smad3-null monocytes and neutrophils were unable to migrate toward TGF-β, suggesting Smad3 is required for migration signal downstream of TGF-β. As shown in Figure 6B, Smad3-null SMCs dose-dependently migrated toward TGF-β at least to a similar extent as

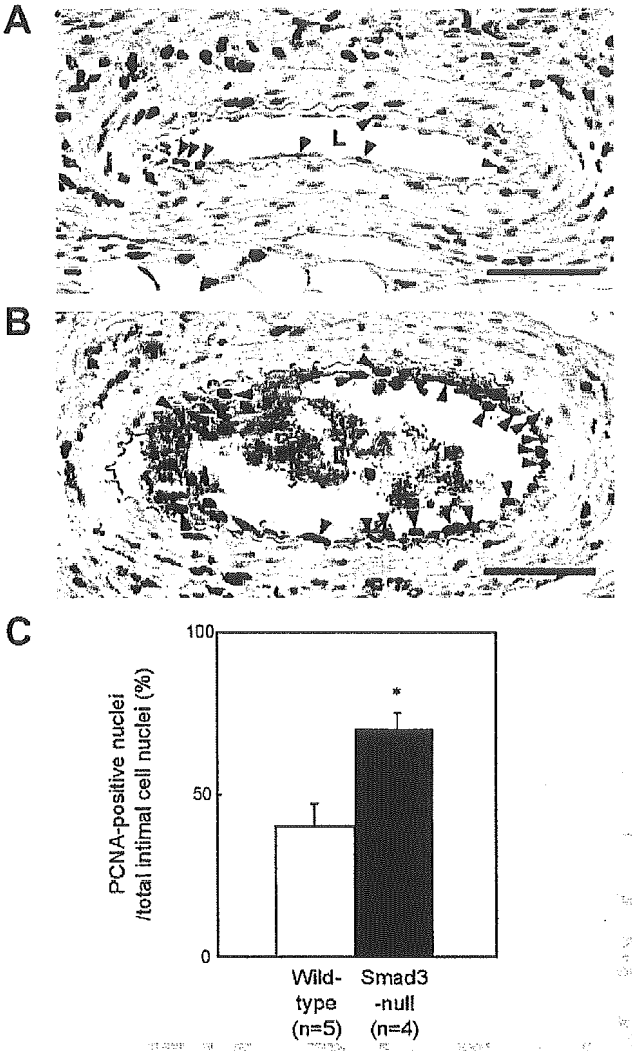

Figure 3. In vivo evaluation of cell proliferation in neointima. Representative anti-PCNA–stained cross sections of femoral arteries from wild-type (A) and Smad3-null (B) mice obtained 1 week after the injury. Arrowheads indicate PCNA-positive cells in intima. C, Ratios of PCNA-positive intimal cell number to total intimal cell number. L indicates vascular lumen. Original magnification ×200; bar=50 μm. *$P<0.05$ compared with the wild type.

wild-type SMCs in a modified Boyden chamber assay. Moreover, Smad3-null cells showed a higher migratory capacity ($P<0.05$) than wild-type cells at 10 ng/mL TGF-β. The result suggests that Smad3-dependent signal is not essential for TGF-β–induced chemotaxis in murine vascular SMCs.

SMCs Require Smad3 for the Regulation of Type I Collagen, Matrix Metalloproteinases, and TIMP-1 by TGF-β

Previous studies suggested that migration of medial SMCs to intima involves extracellular matrix degradation.[38,39] Because TGF-β is implicated in extracellular matrix metabolism through transcriptional regulation of collagens, matrix metalloproteinases (MMPs), and TIMP-1,[7,8] we examined the ability of TGF-β to regulate mRNA expression of these components in wild-type and Smad3-null SMC. Transcript levels of COL1A2, membrane-type matrix metalloproteinase 1 (MT1-MMP), and TIMP-1 were evaluated by real-time quantitative PCR. As shown in Figure 7A, TGF-β time-dependently upregulated mRNA level of COL1A2 in wild-type SMCs with a maximal increase of 3-fold. Induction of COL1A2 by TGF-β was significantly less in Smad3-null SMCs compared with wild-type cells at all time points. TGF-β suppressed mRNA expression of MT-1 MMP, an activator of pro–MMP-2,[40] to 64% of the basal level in wild-type SMCs (Figure 7B). However, MT1-MMP level was not affected by TGF-β in Smad3-null SMCs. Moreover, TGF-β increased TIMP-1 expression by 5-fold over the basal level in wild-type SMCs (Figure 7C), whereas no significant induction was observed in Smad3-null SMCs. Finally, the effect of TGF-β on MMP activity in SMC culture media was examined by gelatin zymography (Figure 7D). The basal gelatinolytic activity of MMP-2 in a serum-free conditioned media was similar for wild-type and Smad3-null SMCs. TGF-β time-dependently suppressed MMP-2 activity in wild-type cells with the maximal suppression of 29% at 24 hours, but it did not show significant effect in Smad3-null SMCs. These results suggest that Smad3 plays an essential role in TGF-β–mediated regulation of type I collagen, MMPs, and TIMP-1 in vascular SMCs.

Discussion

We report six novel findings in this article. First, mice lacking Smad3 showed a significant enhancement of neointimal hyperplasia on endothelial injury compared with corresponding wild-type mice. Second, neointima of Smad3-null mouse after injury contained a larger number of PCNA-positive cells compared with wild-type, indicating an increased proliferative activity of Smad3-null SMCs in vivo. Third, Smad3-null neointima showed higher cell density with reduced collagen area. Fourth, TGF-β–induced growth inhibition was diminished in Smad3-null SMCs in vitro. Fifth, Smad3-null SMCs retained migratory activity toward TGF-β. And finally, Smad3-null SMCs were impaired in induction of type I collagen and TIMP-1 as well as in suppression of MMPs by TGF-β. These results confirm a regulatory role of endogenous Smad3 in vascular remodeling in response to injury.

Enhanced neointimal hyperplasia in Smad3-null mice (Figure 1) lend support to previous reports describing the association of low TGF-β activity either at the ligand or receptor levels with intimal lesion formation. Grainger et al[41] showed that transgenic expression of apolipoprotein(a) promoted SMC proliferation and subsequent development of early vascular lesions by inhibiting proteolytic activation of TGF-β. Conversely, treatment with the antiestrogen tamoxifen increased serum TGF-β_1 levels and suppressed the formation of aortic lesions in mice[42]; a similar effect was also observed in human subjects.[43] McCaffrey et al[19] reported that reduced TβR-II activity due to genomic mutations led to SMC expansion in human atherosclerosis. Moreover, inhibition of TGF-β by use of a soluble type II receptor or a neutralizing antibody accelerated atherosclerosis and induced an unstable plaque phenotype in apoE-deficient mice.[17,18] And our present findings, for the first time, demonstrate a

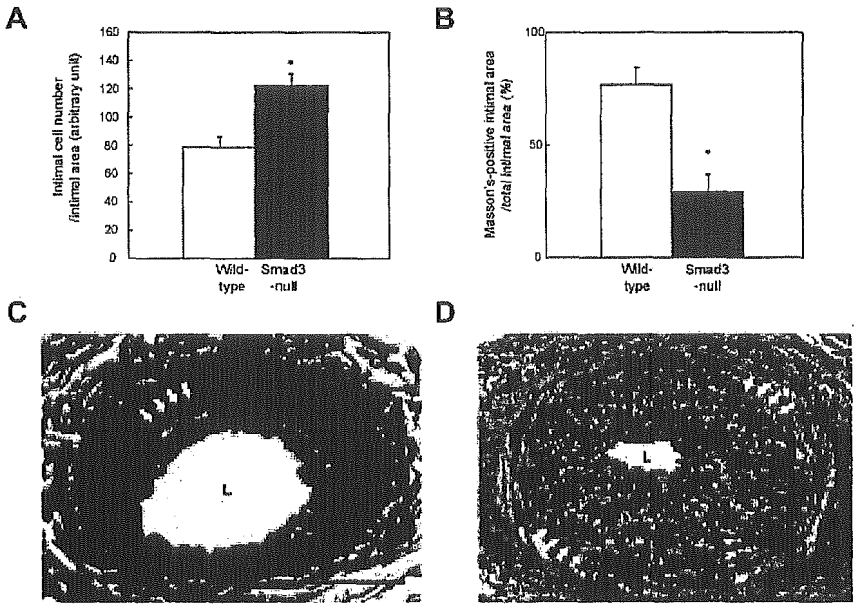

Figure 4. Evaluation of cell density and matrix deposition in neointima. A, Ratios of intimal cell number to total intimal area evaluated on hematoxylin and eosin–stained femoral arterial sections from wild-type (n=7) and Smad3-null (n=6) mice obtained 3 weeks after the injury. B, Ratios of Masson trichrome–positive intimal area to total intimal area in femoral arterial sections from wild-type (n=7) and Smad3-null (n=6) mice 3 weeks after the injury. C and D, Photomicrographs showing the representative Masson trichrome–stained sections of wild-type (C) and Smad3-null (D) femoral arteries. Arrows indicate the positions of the internal elastic lamina. L indicates vascular lumen. Original magnification ×200; bar=50 μm. *$P<0.01$ compared with the wild type.

direct evidence that attenuation of TGF-β signal at the postreceptor level results in enhanced neointimal formation on injury.

Increased PCNA-positive intimal cells in vivo (Figure 3) and defect in TGF-β–induced growth suppression in vitro (Figure 6A) suggest that increased proliferative activity of SMCs contributes to the prominent neointimal formation in Smad3-null mice. Importance of Smad3 in TGF-β–mediated growth inhibition has well been described in other cell types such as αCD-stimulated primary splenocytes and embryonic fibroblasts.[33] Our results verify that Smad3, also in vascular SMCs, plays a major role in growth inhibitory function of TGF-β. It is to be noted that lack of Smad3 did not eliminate TGF-β–induced growth suppression in SMCs (Figure 6A). The residual growth inhibitory activity is likely to depend on another mediator downstream of TGF-β receptors, possibly Smad2.

Ashcroft et al[37] reported that Smad3 is required for TGF-β–induced migration of monocytes, leukocytes, and keratinocytes. Unexpectedly, Smad3-null SMCs were able to migrate toward TGF-β (Figure 6B). The finding suggests that, in contrast to the growth inhibitory function, Smad3-dependent signal is not essential for chemotaxis by TGF-β in murine vascular SMCs. It is therefore likely that the ability of medial SMCs to migrate into intima is preserved in Smad3-null arteries. The signaling pathway responsible for TGF-β–induced SMC motility remains to be elucidated.

TGF-β is known as a potent inducer of ECM deposition. It has been demonstrated that overexpression and intravenous administration of TGF-β caused arterial intimal thickening largely consisted of increased ECM.[10,44] TGF-β exerts fibrogenic activity through enhancement of ECM synthesis as well as inhibition of ECM degradation by downregulating MMP expression and upregulating MMP inhibitors.[6–8] Previous studies, mainly performed on dermal fibroblasts, showed that TGF-β–mediated regulation of many ECM-related genes, such as type I, III, V, and VI collagens, TIMP-1 and MMP-1 was Smad3-dependent.[45–47] In this study, we reported that Smad3-null neointima was rich in SMCs with relatively less matrix deposition compared with wild-type intima, as evaluated by intimal cell density and Masson trichrome staining (Figure 4), confirming a crucial role of Smad3-dependent signals in vascular ECM regulation. Moreover, TGF-β was unable to enhance mRNA expression of COL1A2 and TIMP-1 or suppress MT1-MMP expression in Smad3-null SMCs (Figure 7), establishing Smad3-dependency of these genes in vascular SMCs. Regulation of MMP-2 or gelatinase also seems to depend on Smad3-pathway in SMCs, because TGF-β attenuated MMP-2 activity in the culture media of wild-type but not in Smad3-null SMCs. Because degradation of matrix scaffold by MMPs enables cell movement and general tissue reorganization,[38,39] inability of TGF-β to suppress MMPs in Smad3-null SMCs may facilitate cell migration from media to intima in vivo.[48] Our in vitro finding that Smad3-null SMCs show a higher migration than wild-type at 10 ng/mL TGF-β (Figure 6B) may support this idea. MMP activity uninhibited by TGF-β as well as decreased matrix deposition might also have contributed to enhancement of intimal thickening in Smad3-null mice.

There have been reports on injury models suggesting that TGF-β promotes intimal thickening.[3,9–13,49] The present result that Smad3 deficiency accelerates intimal response to injury appears inconsistent with these results. However, we do not think that our findings contradict to other reports on TGF-β transgene or antagonism. Our model differs from any other previous models in the point it specifically lacks Smad3 signal but not other TGF-β signal components, eg, Smad2 and MAP kinases. Smad3 not only transduces signal downstream of TGF-β, but also plays a major role in signaling of activins,[22,23] other members of the TGF-β superfamily. Activin A is expressed in atherosclerotic lesion[50] and promotes the contractile or nonproliferative phenotype of SMCs,[51] playing a role in stabilization of atherosclerotic plaque. Adenovirus-mediated overexpression of activin A suppresses

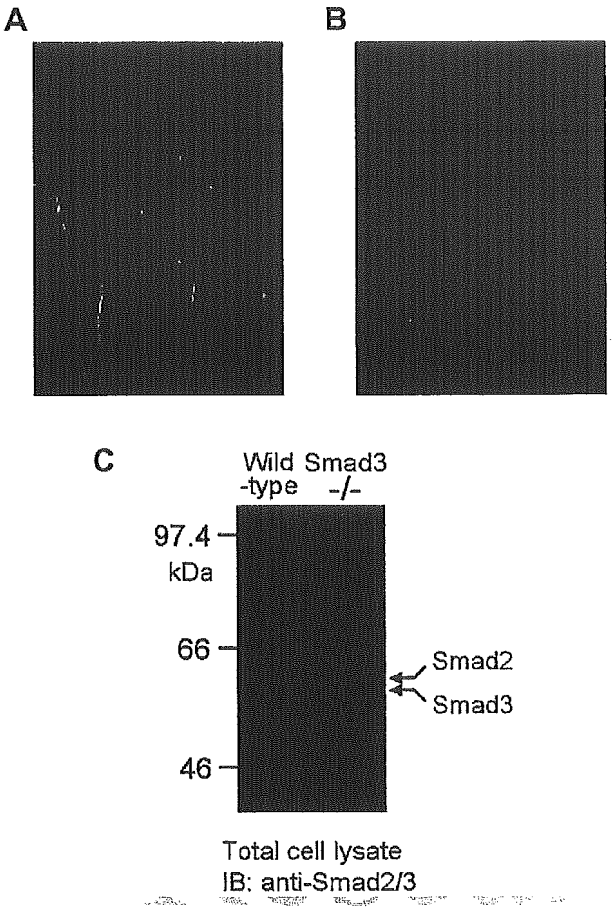

Figure 5. Characterization of cultured mice aortic SMCs. SMCs enzymatically isolated from the aorta of wild-type mice were immunocytochemically stained using anti-SMA (A, green) and anti-SMM (B, red) antibodies, counterstained with DAPI (blue, for nuclei), and subjected to fluorescent microscopy. Original magnification ×200. C, Total cell lysates of wild-type and Smad3-null SMCs were analyzed by SDS-PAGE and subjected to immunoblotting with an anti-Smad2/3 antibody. Migration positions of Smad2 and Smad3 are indicated.

neointimal formation.[51] Although we have not examined the involvement of activin A in the present study, it is assumable that the defect in activin A signal in addition to TGF-β accounts for the drastic neointimal hyperplasia in Smad3-null mice. It is of interest to determine whether specific activation of Smad3 in arterial SMCs in vivo attenuates neointimal hyperplasia. As another possibility, proinflammatory status caused by systemic Smad3 deficiency[27] might have influenced neointimal response. Although our BMT results (Figure 2D through 2F) show that the degree of intimal hyperplasia mainly depends on the origin of blood vessels and not of bone marrow cells, further investigation is needed to elucidate the entire role of inflammation in Smad3-null vascular response.

Finally, overactivation of TGF-β–Smad3 pathway is implicated in various fibrotic diseases involving organs such as skin, lung, liver, and kidney. Molecular agents that block Smad3-dependent TGF-β signal are anticipated as an ideal therapeutic option for these disorders.[46] However, our present results lead us to surmise that systemic suppression of Smad3 signaling can cause undesirable effects in the arteries by facilitating proliferative intimal lesions. Therefore, selective drug-delivery to the affected organs as well as careful monitoring of possible vascular lesions should be considered on clinical application of Smad3 inhibitors for fibrotic diseases.

In conclusion, mice lacking Smad3 developed marked neointimal hyperplasia on injury accompanying modulation of growth and matrix regulation in vascular SMCs. This study documents direct evidence and novel information on the functional significance: a vasculoprotective role of Smad3-dependent TGF-β signaling in response to injury.

Acknowledgments

This study is supported by Grants-in-Aids for Scientific Research from the Ministry of Education, Culture, Sports, Science and Technology, and the Ministry of Health, Labor and Welfare, Japan

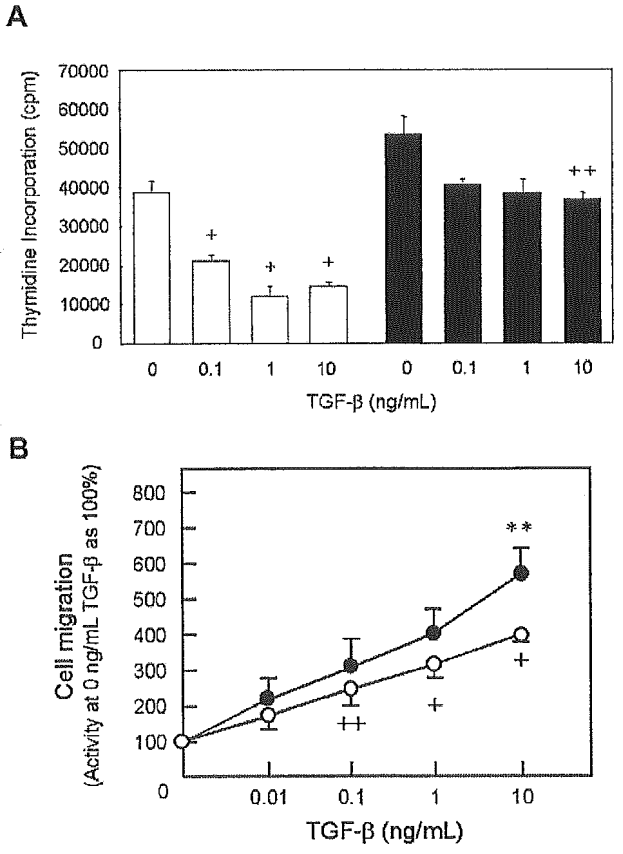

Figure 6. TGF-β–induced growth inhibition and migration of wild-type and Smad3-null SMCs. A, Wild-type (open columns) and Smad3-null (closed columns) SMCs were assayed for TGF-β–induced growth inhibition using ^{3}H-thymidine incorporation. Data are expressed as the means of three separate experiments, each performed in quadruplicate. $+P<0.01$, $++P<0.05$, compared with the value of 0 ng/mL TGF-β. B, Migration of wild-type (open circles) and Smad3-null (closed circles) SMCs toward various doses of TGF-β was measured by use of modified Boyden chamber method. Data represent the percentage of cell numbers relative to those in the absence of TGF-β and are expressed as the means of five separate experiments, each performed in triplicate. $+P<0.01$, $++P<0.05$, compared with the value of 0 ng/mL TGF-β. $**P<0.05$, compared with the value of wild-type at 10 ng/mL TGF-β.

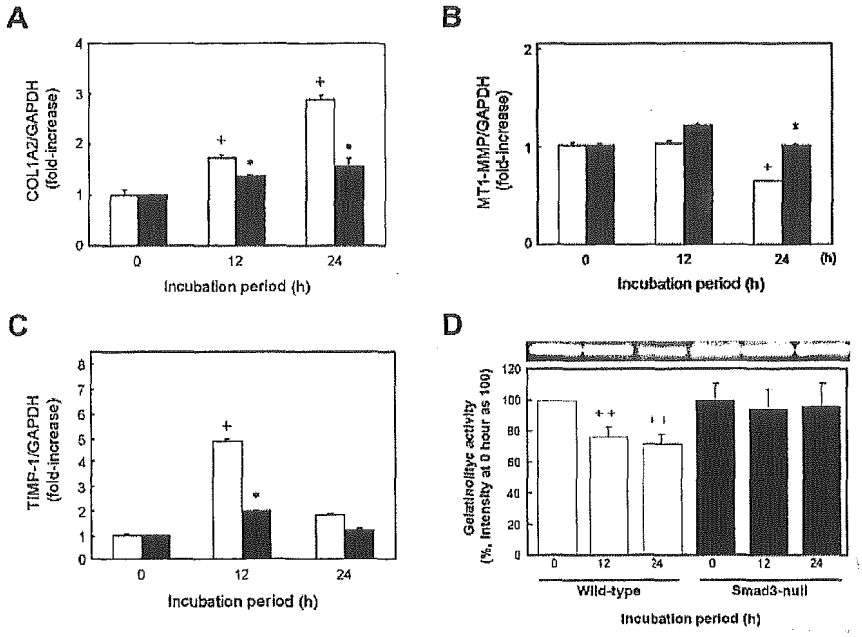

Figure 7. Effect of TGF-β on expression of type I collagen, MMPs, and TIMP-1 in wild-type and Smad3-null SMCs. Transcript levels of COL1A2 (A), MT1-MMP (B), and TIMP-1 (C) in wild-type and Smad3-null SMCs treated with TGF-β. Wild-type (open columns) and Smad3-null (closed columns) SMC were incubated with 10 ng/mL TGF-β for the indicated periods, the total RNA was isolated and used for cDNA synthesis. Quantitative real-time PCR was performed using the SYBR Green PCR Master Mix and analyzed on an ABI PRISM 7000 Sequence Detector System. Data were calculated relative to the value for the cells without TGF-β and are expressed as the means of three separate experiments, each performed in triplicate. +$P<0.01$, compared with the value of 0 hour; *$P<0.01$, compared with the wild type at the same time point. D, MMP-2 gelatinolytic activity in the culture media of wild-type and Smad3-null SMCs treated with TGF-β. Culture media of SMCs incubated with 10 ng/mL TGF-β for the indicated periods was analyzed by gelatin zymogram. Proteolytic degradation of gelatin by MMP was visualized as a translucent band on the dark background. Graph shows the gelatinolytic activity, evaluated by densitometrical scanning of the bands, relative to those of wild-type SMCs at 0 hour. Data were expressed as the means of four separate experiments. ++$P<0.05$, compared with the value of 0 hour.

Heart Foundation, grants from Mitsui Sumitomo Welfare Foundation and NOVARTIS Foundation for Gerontological Research to Koutaro Yokote. We thank Drs A. Roberts and C. Deng (National Institutes of Health, USA) for providing with mice heterozygous for Smad3 disruption, Drs K. Harigaya and M. Higashi for valuable advice on histological examination, Drs K. Sonezaki and T. Tokuyama for fruitful discussion, and A. Takada for technical assistance.

References

1. Roberts AB, Sporn MB. The transforming growth factor-betas. In: Sporn MB, Roberts AB, eds. *Peptide Growth Factors and Their Receptors.* Heidelberg, Germany: Springer-Verlag; 1990;95:419–472.
2. Blobe GC, Schiemann WP, Lodish HF. Role of transforming growth factor β in human disease. *N Engl J Med.* 2000;342:1350–1358.
3. Nikol S, Isner JM, Pickering JG, Kearney M, Leclerc G, Weir L. Expression of transforming growth factor-beta 1 is increased in human vascular restenosis lesions. *J Clin Invest.* 1992;90:1582–1592.
4. Laiho M, Rönnstrand L, Heino J, Decaprio JA, Ludlow JW, Livingston DM, Massagué J. Control of junB and extracellular matrix protein expression by transforming growth factor-beta 1 is independent of simian virus 40 T antigen-sensitive growth-sensitive growth-inhibitory events. *Mol Cell Biol.* 1991;11:972–978.
5. Ignotz RA, Massagué J. Transforming growth factor-beta stimulates the expression of fibronectin and collagen and their incorporation into the extracellular matrix. *J Biol Chem.* 1986;261:4337–4345.
6. Westerhausen DR Jr., Hopkins WE, Billadello JJ. Multiple transforming growth factor- β-inducible elements regulate expression of the plasminogen activator inhibitor type-1 gene in Hep G2 cells. *J Biol Chem.* 1991;266:1092–1100.
7. Eickelberg O, Köhler E, Reichenberger F, Bertschin S, Woodtli T, Erne P, Perruchoud AP, Roth M. Extracellular matrix deposition by primary human lung fibroblasts in response to TGF-β1 and TGF-β3. *Am J Physiol.* 1999;276:L814–L824.
8. Uría JA, Jiménez MG, Balbín M, Freije JM, López-Otín C. Differential effects of transforming growth factor-β on the expression of collagenase-1 and collagenase-3 in human fibroblasts. *J Biol Chem.* 1998;273:9769–9777.
9. Nabel EG, Shum L, Pompili VJ, Yang Z-Y, San H, Shu HB, Liptay S, Gold L, Gordon D, Derynck R, Nabel GJ. Direct transfer of transforming growth factor β1 gene into arteries stimulates fibrocellular hyperplasia. *Proc Natl Acad Sci U S A.* 1993;90:10759–10763.
10. Schulick AH, Taylor AJ, Zuo W, Qiu C-B, Dong G, Woodward RN, Agah R, Roberts AB, Virmani R, Dichek DA. Overexpression of transforming growth factor β1 in arterial endothelium causes hyperplasia, apoptosis, and cartilaginous metaplasia. *Proc Natl Acad Sci U S A.* 1998;95:6983–6988.
11. Wolf YG, Rasmussen LM, Rouslahti E. Antibodies against transforming growth factor-b1 suppresses intimal hyperplasia in a rat model. *J Clin Invest.* 1994;93:1172–1178.
12. Kingston PA, Sinha S, David A, Castro MG, Lowenstein PR, Heagerty AM. Adenovirus-mediated gene transfer of a secreted transforming growth factor-β type II receptor inhibits luminal loss and constrictive remodeling after coronary angioplasty and enhances adventitial collagen deposition. *Circulation.* 2001;104:2595–2601.
13. Yamamoto K, Morishita R, Tomita N, Shimozato T, Nakagami H, Kikuchi A, Aoki M, Higaki J, Kaneda Y, Ogihara T. Ribozyme oligonucleotides against transforming growth factor-β inhibited neointimal formation after vascular injury in rat model: potential application of ribozyme strategy to treat cardiovascular disease. *Circulation.* 2000;102:1308–1314.
14. Morisaki N, Kawano M, Koyama N, Koshikawa T, Umemiya K, Saito Y, Yoshida S. Effects of transforming growth factor-beta 1 on growth of aortic smooth muscle cells. Influences of interaction with growth factors, cell state, cell phenotype, and cell cycle. *Atherosclerosis.* 1991;88:227–234.
15. Goodman LV, Majack RA. Vascular smooth muscle cells express distinct transforming growth factor-β receptor phenotypes as a function of cell density in culture. *J Biol Chem.* 1989;264:5241–5244.
16. Lutgens E, Gijbels M, Smook M, Heeringa P, Gotwals P, Koteliansky VE, Daemen MJ. Transforming growth factor-β mediates balance between inflammation and fibrosis during plaque progression. *Arterioscler Thromb Vasc Biol.* 2002;22:975–982.
17. Mallat Z, Gojova A, Marchiol-Fournigault C, Esposito B, Kamaté C, Merval R, Fradelizi D, Tedgui A. Inhibition of transforming growth factor-β signaling accelerates atherosclerosis and induces an unstable plaque phenotype in mice. *Circ Res.* 2001;89:930–934.
18. Robertson AK, Rudling M, Zhou X, Gorelik L, Flavell RA, Hansson GK. Disruption of TGF-beta signaling in T cells accelerates atherosclerosis. *J Clin Invest.* 2003;112:1342–1350.
19. McCaffrey TA, Du B, Consigli S, Szabo P, Bray PJ, Hartner L, Weksler BB, Sanborn TA, Bergman G, Bush HL Jr. Genomic instability in the type II TGF-β1 receptor gene in atherosclerotic and restenotic vascular cells. *J Clin Invest.* 1997;100:2182–2188.

20. McCaffrey TA, Du B, Fu C, Bray PJ, Sanborn TA, Deutsch E, Tarazona N, Shaknovitch A, Newman G, Patterson C, Bush HL Jr. The expression of TGF-β receptors in human atherosclerosis: evidence for acquired resistance to apoptosis due to receptor imbalance. *J Mol Cell Cardiol.* 1999;31:1627–1642.
21. Grainger DJ, Kemp PR, Metcalfe JC, Liu AC, Lawn RM, Williams NR, Grace AA, Schofield PM, Chauhan A. The serum concentration of active transforming growth factor-β is severely depressed in advanced atherosclerosis. *Nat Med.* 1995;1:74–79.
22. Heldin C-H, Miyazono K, ten Dijke P. TGF- β signalling from cell membrane to nucleus through SMAD proteins. *Nature.* 1997;390: 465–471.
23. Massagué J, Chen Y-G. Controlling TGF-β signaling. *Genes Dev* 2000; 14:627–644.
24. Sirard C, de la Pompa JL, Elia A, Itie A, Mirtsos C, Cheung A, Hahn S, Wakeham A, Schwartz L, Kern SE, Rossant J, Mak TW. The tumor suppressor gene Smad4/Dpc4 is required for gastrulation and later for anterior development of the mouse embryo. *Genes Dev.* 1998;12: 107–119.
25. Yang X, Li C, Xu X, Deng C. The tumor suppressor SMAD4/DPC4 is essential for epiblast proliferation and mesoderm induction in mice. *Proc Natl Acad Sci U S A.* 1998;95:3667–3672.
26. Waldrip WR, Bikoff EK, Hoodless PA, Wrana JL, Robertson EJ. Smad2 signaling in extraembryonic tissues determines anterior-posterior polarity of the early mouse embryo. *Cell.* 1998;92:797–808.
27. Yang X, Letterio JJ, Lechleider RJ, Chen L, Hayman R, Gu H, Roberts AB, Deng C. Targeted disruption of SMAD3 results in impaired mucosal immunity and diminished T cell responsiveness to TGF-beta. *EMBO J.* 1999;18:1280–1291.
28. Kikuchi S, Umemura K, Kondo K, Saniabadi AR, Nakashima M. Photochemically induced endothelial injury in the mouse as a screening model for inhibitors of vascular intimal thickening. *Arterioscler Thromb Vasc Biol.* 1998;18:1069–1078.
29. Yamashita K, Sakamoto A, Ohkubo Y, Arima M, Hatano M, Kuroda Y, Tokuhisa T. C-fos overexpression in splenic B cells augments development of marginal zone B cells. *Mol Immunol.* 2005;42:617–625.
30. Ohmi K, Masuda T, Yamaguchi H, Sakurai T, Kudo Y, Katsuki M, Nonomura Y. A novel aortic smooth muscle cell line obtained from p53 knock out mice expresses several differentiation characteristics. *Biochem Biophys Res Commun.* 1997;238:154–158.
31. Hasegawa K, Arakawa E, Oda S, Yanai N, Obinata M, Matsuda Y. Novel smooth muscle cell lines from transgenic mice harboring temperature-sensitive SV40 large T-antigen gene: temperature-dependent expression of smooth muscle myosin heavy chain-1 and calponin genes. *J Mol Cell Cardiol.* 1997;29:2177–2186.
32. Yokote K, Mori S, Hansen K, McGlade J, Pawson T, Heldin CH, Claesson-Welsh L. Direct interaction between Shc and the platelet-derived growth factor β-receptor. *J Biol Chem.* 1994;269:15337–15343.
33. Datto MB, Frederick JP, Pan L, Borton AJ, Zhuang Y, Wang XF. Targeted disruption of Smad3 reveals an essential role in transforming growth factor β–mediated signal transduction. *Mol Cell Biol.* 1999;19: 2495–2504.
34. Yokote K, Mori S, Siegbahn A, Ronnstrand L, Wernstedt C, Heldin CH, Claesson-Welsh L. Structural determinants in the platelet-derived growth factor α-receptor implicated in modulation of chemotaxis. *J Biol Chem.* 1996;271:5101–5111.
35. Fischer-Dzoga K, Dimitrievich GS, Griem ML. Radiosensitivity of vascular tissue, II: differential radiosensitivity of aortic cells in vitro. *Radiat Res.* 1984;99:536–546.
36. Waksman R, Robinson KA, Crocker IR, Gravanis MB, Cipolla GD, King SB 3rd. Endovascular low-dose irradiation inhibits neointima formation after coronary artery balloon injury in swine: a possible role for radiation therapy in restenosis prevention. *Circulation.* 1995;91:1533–1539.
37. Ashcroft GS, Yang X, Glick AB, Weinstein M, Letterio JL, Mizel DE, Anzano M, Greenwell-Wild T, Wahl SM, Deng C, Roberts AB. Mice lacking Smad3 show accelerated wound healing and an impaired local inflammatory response. *Nat Cell Biol.* 1999;1:260–266.
38. Lijnen HR, Soloway P, Collen D. Tissue inhibitor of matrix metalloproteinases-1 impairs arterial neointima formation after vascular injury in mice. *Circ Res.* 1999;85:1186–1191.
39. Galis ZS, Johnson C, Godin D, Magid R, Shipley JM, Senior RM, Ivan E. Targeted disruption of the matrix metalloproteinase-9 gene impairs smooth muscle cell migration and geometrical arterial remodeling. *Circ Res.* 2002;91:852–859.
40. Sato H, Takino T, Kinoshita T, Imai K, Okada Y, Stetler Stevenson WG, Seiki M. Cell surface binding and activation of gelatinase A induced by expression of membrane-type-1-matrix metalloproteinase (MT1-MMP). *FEBS Lett.* 1996;385:238–240.
41. Grainger DJ, Kemp PR, Liu AC, Lawn RM, Metcalfe JC. Activation of transforming growth factor-beta is inhibited in transgenic apolipoprotein(a) mice. *Nature.* 1994;370:460–462.
42. Grainger DJ, Witchell CM, Metcalfe JC. Tamoxifen elevates transforming growth factor-beta and suppresses diet-induced formation of lipid lesions in mouse aorta. *Nat Med.* 1995;1:1067–1073.
43. McDonald CC, Alexander FE, Whyte BW, Forrest AP, Stewart HJ. Cardiac and vascular morbidity in women receiving adjuvant tamoxifen for breast cancer in a randomised trial. The Scottish Cancer Trials Breast Group. *BMJ.* 1995;311:977–980.
44. Kanzaki T, Tamura K, Takahashi K, Saito Y, Akikusa B, Oohashi H, Kasayuki N, Ueda M, Morisaki N. In vivo effect of TGF-β1: enhanced intimal thickening by administration of TGF-β1 in rabbit arteries injured with a balloon catheter. *Arterioscler Thromb Vasc Biol.* 1995;15: 1951–1957.
45. Yuan W, Varga J. Transforming growth factor- β repression of matrix metalloproteinase-1 in dermal fibroblasts involves Smad3. *J Biol Chem.* 2001;276:38502–38510.
46. Xu G, Chakraborty C, Lala PK. Reconstitution of Smad3 restores TGF-β response of tissue inhibitor of metalloprotease-1 upregulation in human choriocarcinoma cells. *Biochem Biophys Res Commun.* 2003;300: 383–390.
47. Flanders KC. Smad3 as a mediator of the fibrotic response. *Int J Exp Pathol.* 2004;85:47–64.
48. Galis ZS, Khatri JJ. Matrix metalloproteinases in vascular remodeling and atherogenesis: the good, the bad, and the ugly. *Circ Res.* 2002;90: 251–262.
49. Chung IM, Ueno H, Pak YK, Kim JW, Choi DH, Shin GJ, Yang WI, Jang Y. Catheter-based adenovirus-mediated local intravascular gene delivery of a soluble TGF-β type II receptor using an infiltrator in porcine coronary arteries: efficacy and complications. *Exp Mol Me.* 2002;34: 299–307.
50. Inoue S, Orimo A, Hosoi T, Ikegami A, Kozaki K, Ouchi Y, Nomura S, Muramatsu M, Orimo H. Demonstration of activin-A in arteriosclerotic lesions. *Biochem Biophys Res Commun.* 1994;205:441–448.
51. Engelse MA, Neele JM, van Achterberg TA, van Aken BE, van Schaik RH, Pannekoek H, de Vries CJ. Human activin-A is expressed in the atherosclerotic lesion and promotes the contractile phenotype of smooth muscle cells. *Circ Res.* 1999;85:931–939.

Our report is, to the best of our knowledge, the first one describing the effects of obesity surgery in type 1 diabetes. In our opinion, gastric bypass surgery, which is being performed increasingly often (~100,000 operations in the U.S. annually [10]) in obese individuals, also with type 2 diabetes (4–8), is a feasible, safe, and effective method of weight reduction in young type 1 diabetic patients with severe obesity and comorbidities leading to metabolic syndrome (e.g., hypertension, hyperlipidemia) (11). In our patients, surgery-induced weight loss was also associated with a decrease in insulin requirement per kilogram of body weight (0.60 to 0.53 IU/kg in the first patient and from 0.95 to 0.83 IU/kg in the second patient). This observation may suggest the presence of clinically significant insulin resistance in severely obese type 1 diabetic subjects (12), which was subsequently reduced once weight loss occurred. Importantly, neither of the patients had any significant hypoglycemic episodes after the surgery, despite considerable reduction in HbA_{1c} level and apparent increase in insulin sensitivity.

In conclusion, gastric bypass surgery not only leads to a significant and maintained weight loss in type 1 diabetic patients, but also results in remarkable improvement in metabolic control (absolute reduction in HbA_{1c} of 3–4%) and concomitant disorders. Interestingly, the need for constant intensive insulin therapy in these patients had no detrimental influence on weight loss as an effect of obesity surgery. Both patients lost 50–60% of their excessive body weight during the follow-up period, which is also the rate reported in nondiabetic subjects (4,5,7).

LESZEK CZUPRYNIAK, MD, PHD[1]
JANUSZ STRZELCZYK, MD, PHD[2]
KATARZYNA CYPRYK, MD, PHD[3]
MACIEJ PAWLOWSKI, MD[1]
DARIUSZ SZYMANSKI, MD, PHD[2]
ANDRZEJ LEWINSKI, MD, PHD[3]
JERZY LOBA, MD, PHD[1]

From the [1]Department of Diabetology and Metabolic Diseases, Medical University of Lodz, Lodz, Poland; the [2]Department of General and Transplant Surgery, Medical University of Lodz, Lodz, Poland; and the [3]Department of Endocrinology and Isotope Therapy, Polish Mother's Memorial Hospital Research Institute, Medical University of Lodz, Lodz, Poland.

Address correspondence to Leszek Czupryniak, MD, PHD, Department of Diabetology and Metabolic Diseases, Barlicki University Hospital, No. 1, Ul, Kopcinskiego 22, 90-153 Lodz, Poland. E-mail: bigosik@poczta.onet.pl.

References

1. Greenfield JR, Samaras K, Campbell LV, Chisholm DJ: Type 1 diabetes is not associated with increased central abdominal obesity (Letter). *Diabetes Care* 26:2703, 2003
2. Sibley SD, Palmer JP, Hirsch IB, Brunzell JD: Visceral obesity, hepatic lipase activity, and dyslipidemia in type 1 diabetes. *J Clin Endocrinol Metab* 88:3379–3384, 2003
3. Kabadi UM, Vora A, Kabadi M: Hyperinsulinemia and central adiposity: influence of chronic insulin therapy in type 1 diabetes (Letter). *Diabetes Care* 23:1024–1025, 2000
4. Fobi MA, Lee H, Holness R, Cabinda D: Gastric bypass operation for obesity. *World J Surg* 22:925–935, 1998
5. Pories WJ, Swanson MS, MacDonald KG Jr, Long SB, Morris P, Brown BM, Bakarat HA, deRamon RA, Israel G, Dolezal JM, Dohm GL: Who would have thought it? An operation proves to be the most effective therapy for adult-onset diabetes mellitus. *Ann Surg* 222:339–350, 1995
6. Smith SC, Edwards CB, Goodman GN: Changes in diabetic management after Roux-en-Y gastric bypass. *Obes Surg* 6: 345–348, 1996
7. Eisenberg D, Bell RL: The impact of bariatric surgery on severely obese patients with diabetes. *Diabetes Spectrum* 16:240–245, 2003
8. Clements RH, Gonzalez QH, Long CI, Wittert G, Laws HL: Hormonal changes after Roux-en-Y gastric bypass for morbid obesity and the control of type-II diabetes mellitus. *Am Surg* 70:1–5, 2004
9. Strzelczyk J, Czupryniak L, Loba J, Wasiak J: The use of polypropylene mesh in midline incision closure following gastric by-pass surgery reduces the risk of postoperative hernia. *Langenbecks Arch Surg* 387:294–297, 2002
10. Brody JE: Surgical alternatives for the truly overwieght. *New York Times*, 31 December 2002: Sect. F, p. 7
11. Expert Panel on Detection, Evaluation, and Treatment of High Blood Cholesterol in Adults: Executive summary of the Third Report of the National Cholesterol Education Programme (NCAP) Expert Panel on Detection, Evaluation, and Treatment of High Blood Cholesterol in Adults (Adult Treatment Panel III). *JAMA* 285:2486–2497, 2001
12. Greenfield JR, Samaras K, Chisholm DJ: Insulin resistance, intra-abdominal fat, cardiovascular risk factors, and androgens in healthy young women with type 1 diabetes mellitus. *J Clin Endocrinol Metab* 87:1036–1040, 2002

Dysadipocytokinemia in Werner Syndrome and Its Recovery by Treatment With Pioglitazone

Werner syndrome (WS) (Mendelian Inheritance in Man no. 277700) is an autosomal recessive disorder known for progeroid phenotypes including graying and loss of hair, juvenile cataracts, insulin-resistant diabetes, skin atrophy, premature atherosclerosis, and cancer (1). Mutations in *WRN*, a RECQ family DNA/RNA helicase gene, have been identified to cause this disease. The mechanism for insulin resistance in WS remains to be elucidated.

Adipocytes secrete a number of hormones (or adipocytokines), such as tumor necrosis factor-α (TNF-α), leptin, adiponectin, and resistin, thereby regulating insulin sensitivity (2). WS patients typically show the lipoatrophic skinny extremities with an obese trunk (1). The accumulated intra-abdominal visceral fat (3) suggests an altered production of adipocytokines.

To investigate the role of adipocytokines in the pathophysiology of WS, we examined the serum levels of TNF-α and adiponectin in WS. Sera sampled from 24 WS patients (14 men and 10 women; 16 with and 8 without diabetes) proven to be homozygous for *WRN* mutations, and 40 age- and sex-matched normoglycemic healthy volunteers were assayed after informed consent was obtained. Age (43 ± 8.1 vs. 41.6 ± 7.5 years) and BMI (19.4 ± 1.9 vs. 18.8 ± 2.0 kg/m^2) were similar for diabetic and nondiabetic WS patients.

The serum level of TNF-α, a mediator of insulin resistance, was significantly elevated in WS regardless of having diabetes (21.8 ± 8.7 pg/ml, $P < 0.0001$ by Mann-Whitney test) or not having diabetes (14.0 ± 3.2 pg/ml, $P = 0.002$) compared with the healthy control group (6.05 ± 3.0 pg/ml). Adiponectin levels in diabetic WS patients (3.1 ± 2.9 μg/ml) was significantly lower than in nondiabetic WS patients (11.6 ± 9.2 μg/ml, $P = 0.006$) or control subjects (14.4 ± 8.8 μg/ml, $P < 0.0001$). The growing evidence indicates insulin sensitizing as well as antiatherogenic actions of adiponectin and the association of decreased serum adiponectin with insulin resistance, obe-

sity, and type 2 diabetes (2,4). Although WS patients are usually not obese by the definition of BMI, the visceral fat specifically accumulated by an unknown mechanism (3) might cause high TNF-α and low adiponectin levels, characteristics similar to morbid obesity.

We recently reported the successful improvement of glycemic control and insulin sensitivity by pioglitazone in diabetic WS patients (5). Therefore, we next assessed adipocytokines before and after 16 weeks on pioglitazone (15 mg/day) in three diabetic WS patients. The treatment significantly elevated adiponectin levels from 2.57 ± 1.36 to 7.07 ± 2.48 μg/ml ($P = 0.03$ by paired t test). TNF-α and HbA_{1c} levels showed a tendency to decline from 16.1 ± 4.75 to 3.53 ± 0.58 pg/ml ($P = 0.052$) and from 7.7 ± 0.6 to 6.4 ± 0.5% ($P = 0.17$), respectively.

To our knowledge, this is the first study to examine serum adipocytokine levels in WS patients. Reduced insulin sensitivity with increased visceral adiposity is the hallmark of both WS and normal aging. Because pioglitazone achieved improvement of glycemic control as well as correction of adiponectin and TNF-α levels, these cytokines are likely to be at least in part responsible for insulin resistance in WS. Adipocyte function may be a key element linking *WRN* mutation and the metabolic abnormalities observed in WS. It is also of our interest to know whether pioglitazone and other thiazolidinediones can prevent or delay the onset of diabetes in WS by modulating adipocytokines. Our present findings raise a possibility that pioglitazone could extend the lifespan of WS patients by improving metabolism and preventing early cardiovascular death.

KOUTARO YOKOTE, MD[1,2]
KAZUO HARA, MD[3]
SEIJIRO MORI, MD[1,2]
TAKASHI KADOWAKI, MD[3]
YASUSHI SAITO, MD[1,2]
MAKOTO GOTO, MD[4,5]

From the [1]Division of Endocrinology and Metabolism, Department of Internal Medicine, Chiba University Hospital, Chiba City, Japan; the [2]Department of Clinical Cell Biology, Chiba University Graduate School of Medicine, Chiba City, Japan; the [3]Department of Metabolic Diseases, Graduate School of Medicine, University of Tokyo, Tokyo, Japan; the [4]Department of Rheumatology, Tokyo Metropolitan Otsuka Hospital, Tokyo, Japan; and the [5]Institute of Bioengineering, Toin Yokohama University, Yokohama, Japan.

Address correspondence to Koutaro Yokote, MD, Division of Endocrinology and Metabolism, Department of Internal Medicine, Chiba University Hospital, 1-8-1 Inohana, Chuo-ku, Chiba 260-8670, Japan. E-mail: kyokote-cib@umin.ac.jp.

Acknowledgments— We thank Dr. R.W. Miller (National Cancer Institute) for helpful comments. This work was supported in part by the grants from the Japanese Ministry of Education, Science and Sports and the Ministry of Health, Labor and Welfare.

References

1. Goto M: Clinical characteristics of Werner syndrome and other premature aging syndromes: pattern of aging in progeroid syndromes. In *From Premature Gray Hair to Helicase-Werner Syndrome: Implication for Aging and Cancer*. Goto M, Miller RW, Eds. Basel, Karger, 2001, p. 27–39
2. Yamauchi T, Kamon J, Waki H, Terauchi Y, Kubota N, Hara K, Mori Y, Ide T, Murakami K, Tsuboyama-Kasaoka N, Ezaki O, Akanuma Y, Gavrilova O, Vinson C, Reitman ML, Kagechika H, Shudo K, Yoda M, Nakano Y, Tobe K, Nagai R, Kimura S, Tomita M, Froguel P, Kadowaki T: The fat-derived hormone adiponectin reverses insulin resistance associated with both lipoatrophy and obesity. *Nat Med* 7:941–946, 2001
3. Mori S, Murano S, Yokote K, Takemoto M, Asaumi S, Take A, Saito Y: Enhanced intra-abdominal visceral fat accumulation in patients with Werner's syndrome. *Int J Obes Relat Metab Disord* 25:292–295, 2001
4. Daimon M, Oizumi T, Saitoh T, Yamaguchi H, Hirata A, Ohnuma H, Igarashi M, Eguchi H, Manaka H, Tominaga M: Decreased serum levels of adiponectin are a risk factor for the progression to type 2 diabetes in the Japanese population. *Diabetes Care* 26:2015–2020, 2003
5. Yokote K, Honjo S, Kobayashi K, Fujimoto M, Kawamura H, Mori S, Saito Y: Metabolic improvement and abdominal fat redistribution in Werner syndrome by pioglitazone (Letter). 52:1582–1583, 2004

Effect of α-Linolenic Acid–Containing Linseed Oil on Coagulation in Type 2 Diabetes

Blood coagulation in diabetes is known to be increased (1,2). Because levels of n-3 and n-6 polyunsaturated fatty acids (PUFAs) influence the parameters of blood coagulation, the aim of this study was to determine the effects of n-3 PUFA supplementation on coagulation and fibrinolytic factors in type 2 diabetic subjects. While it is not clear what the appropriate intake ratio of n-6 to n-3 PUFAs should be for diabetic subjects, it is known that the dietary intake ratio of n-6 to n-3 PUFAs is roughly 4:1 in Japanese subjects (3).

Ten subjects (six women and four men, average age 59.6 years) with type 2 diabetes participated in this study as inpatients. Their average BMI and HbA_{1c} values were 20.9 ± 3.8 kg/m^2 and 10.8 ± 1.1%, respectively. Their daily energy intake during the course of the study was 1,490 ± 166 kcal. After 2 weeks on the control diet, our subjects were placed on a diet in which 5 g linseed oil was added (in salads, miso soup, etc., without heating) in exchange for 5 g cooking oil. The ratio of PUFAs to saturated fatty acids in the subjects' prestudy and study diets were 1.2 and 1.6, respectively, while the ratios of n-6 to n-3 PUFAs in their prestudy and study diets were 3.6 and 1.5, respectively. Blood samples were collected before and 14 days after initiation of the study. Plasmin α2-plasmin inhibitor complex (PPI) level and plasminogen activator inhibitor-1 (PAI-1) activity in plasma was measured using a latex photometric immunoassay, while thrombin antithrombin III complex (TAT) level was measured using an enzyme-linked immunoassay. Differences in these parameters obtained at the start and end of the study were analyzed using a paired t test; values were considered to be significant if the P value was <0.05. Values are expressed as the mean ± SD.

After 2 weeks on a linseed oil–supplemented diet, PPI level, PAI-1 activity, and TAT level fell significantly (0.72 ± 0.19 vs. 0.47 ± 0.14 μg/ml, $P = 0.0009$; 73.3 ± 37.5 vs. 51.6 ± 25.0 ng/ml, $P = 0.02$; and 9.6 ± 9.1 vs. 2.5 ± 1.1 ng/ml, $P = 0.04$; respectively).

Boberg et al. (4) reported that PAI-1 activity was increased in type 2 diabetic subjects after supplementation of their diet with 10 g eicosapentaenoic acid. Kelly et al. (5) reported that a diet containing flaxseed oil (60% α-linolenic acid) did not alter indexes of blood coagulation, i.e., bleeding time, prothrombin time, and partial prothrombin time. Chan et al. (6) showed that altering the dietary n-6–to–n-3 PUFA ratio had no effect on

clinical trials or meta-analysis. The epidemiological literature did not need a clinical trial to conclude that smoking causes lung cancer. In the case of propoxyphene, clinical trials have already indicated its lack of efficacy advantages over other alternatives, and epidemiological studies have shown its potential to increase risk of fractures in addition to other known side effects. We appreciate Dr. Morton's clinical experience of treating many patients with propoxyphene and achieving acceptable analgesic efficacy with only rare adverse experiences over the last 25 years. But, again, this by itself is not rigorous scientific evidence of the efficacy and safety of propoxyphene in elderly patients; in fact, in epidemiological terms, Dr. Morton's own clinical experience can be considered an example of only a case series study design.

Sachin J. Kamal-Bahl, PhD
Jalpa A. Doshi, PhD
Bruce C. Stuart, PhD
Becky A. Briesacher, PhD
University of Maryland Baltimore
School of Pharmacy
Baltimore, MD

REFERENCES

1. Kamal-Bahl S, Doshi JA, Stuart B et al. Propoxyphene use by community-dwelling and institutionalized elderly Medicare beneficiaries. J Am Geriatr Soc 2003;51:1099–1104.
2. Chronic Pain Management in the Long-Term Care Setting. Columbia, MD: American Medical Directors Association, 1999.
3. American Geriatrics Society. The management of chronic pain in older persons. Clinical practice guidelines. J Am Geriatr Soc 1998;46:635–651.
4. Frenchman BI. Treatment options for the elderly patient with mild to moderate pain. Consultant Pharmacist 1998;14:12–18.
5. Beers MH, Ouslander JG, Rollingher I et al. Explicit criteria for determining inappropriate medication use in nursing home residents. UCLA Division of Geriatric Medicine. Arch Intern Med 1991;151:1825–1832.
6. Beers MH. Explicit criteria for determining potentially inappropriate medication use by the elderly. An update. Arch Intern Med 1997;157:1531–1536.
7. Zhan C, Sangl J, Bierman AS et al. Potentially inappropriate medication use in the community-dwelling elderly: Findings from the 1996 Medical Expenditure Panel Survey. JAMA 2001;286:2823–2829.
8. Fick D, Cooper JW, Wade WE et al. Updating the Beers criteria for potentially inappropriate medication use in older adults: Results of a U.S. consensus panel of experts. Arch Intern Med 2003;163:2716–2724.
9. Ensrud KE, Blackwell TL, Mangione CM et al. Central nervous system active medications and risk for falls in older women. J Am Geriatr Soc 2002;50: 1629–1637.
10. Ensrud KE, Blackwell TL, Mangione CM et al. Central nervous system active medications and risk for fractures in older women. Arch Intern Med 2003;163: 949–957.
11. Shorr RI, Griffin MR, Daugherty JR et al. Opioid analgesics and the risk of hip fracture in the elderly: Codeine and propoxyphene. J Gerontol 1992;47: M111–M115.
12. Guo Z, Wills P, Viitanen M et al. Cognitive impairment, drug use, and the risk of hip fracture in persons over 75 years old: A community-based prospective study. Am J Epidemiol 1998;148:887–892.
13. Kelly KD, Pickett W, Yiannakoulias N et al. Medication use and falls in community-dwelling older persons. Age Ageing 2003;32:503–509.

METABOLIC IMPROVEMENT AND ABDOMINAL FAT REDISTRIBUTION IN WERNER SYNDROME BY PIOGLITAZONE

To the Editor: Werner syndrome is a rare autosomal recessive disorder known for its premature aging phenotype including loss of hair, cataracts, atrophy of peripheral soft tissue, diabetes mellitus, and atherosclerosis. Mutations in the deoxyribonucleic acid (DNA) helicase gene have been identified as the cause of this disease.[1] One common feature of Werner syndrome is insulin resistance, but the mechanism by which insulin resistance occurs in this syndrome is unknown. We have previously described that visceral fat accumulation is strongly associated with insulin resistance in Werner syndrome.[2] We report a case of Werner syndrome in which administration of pioglitazone, a thiazolidinedione derivative, improved insulin sensitivity, glucose tolerance, lipid metabolism, and abdominal fat distribution.

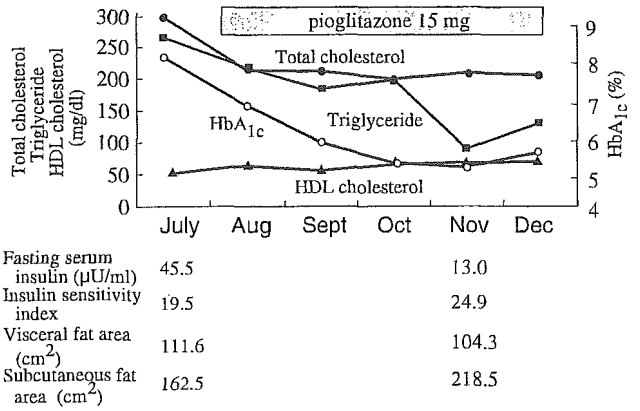

Fasting serum insulin (μU/ml)	45.5	13.0
Insulin sensitivity index	19.5	24.9
Visceral fat area (cm^2)	111.6	104.3
Subcutaneous fat area (cm^2)	162.5	218.5

Fig. 1 Metabolic parameters and abdominal fat areas before and during pioglitazone treatment. HDL = high-density lipoprotein; Hb = hemoglobin.

A 46-year old woman with Werner syndrome came to our hospital for glycemic control. After obtaining written informed consent, we analyzed genomic DNA from peripheral leukocytes, which revealed that the patient was homozygote for type 4 mutation in the Werner helicase gene.[3] She was thin (body mass index = 16.5 kg/m^2) but had accumulated visceral fat in excess, as determined using a computed tomography scan at the umbilical level (visceral fat area = 111.6 cm^2, normal range for Japanese women <90).[4] She also had type IIb hyperlipidemia according to World Health Organization classification. She had significant insulin resistance, as determined using an insulin sensitivity index calculated from the value of steady state plasma glucose (19.4, normal range 55–162).[5] After 1 week of treatment with diet, pioglitazone 15 mg daily was initiated. After 16 weeks of pioglitazone treatment, the patient's fasting plasma glucose had decreased from 198 mg/dL to 115 mg/dL, glycated hemoglobin A1c from 8.4% to 5.9% (normal = 5.9% or less), serum total cholesterol from 270 mg/dL to 209 mg/dL (normal = 130–220 mg/dL), serum triglyceride from 301 mg/dL to 90 mg/dL (normal = 80–150 mg/dL), and serum high-density lipoprotein-cholesterol increased from 52 mg/dL to 64 mg/dL (normal ≥ 40 mg/dL). Fasting serum insulin decreased from 45.5 μU/mL to 13.0 μU/mL (normal = 6–26 μU/mL), and insulin sensitivity index had improved to 24.9 (Figure 1, July to November). Although the patient gained weight, from 35.9 kg to 39.0 kg, during the period, her visceral fat area (V) decreased to 104.3 cm^2. In contrast, abdominal subcutaneous fat area (S) increased from 162.5 cm^2 to 218.5 cm^2. As a result, her V/S ratio decreased from 0.69 to 0.48 (normal range for Japanese